Published in final edited form as:

*Clin Cancer Res*. 2018 December 01; 24(23): 6078–6097. doi:10.1158/1078-0432.CCR-18-0693.

# Pericytes elicit resistance to vemurafenib and sorafenib therapy in thyroid carcinoma via the TSP-1/TGFβ1 axis

**Alessandro Prete**[#1,2], **Agnes S. Lo**[#3], **Peter M. Sadow**[4], **Swati S. Bhasin**[5], **Zeus A. Antonello**[1,2], **Danica M. Vodopivec**[1,2], **Soumya Ullas**[6], **Jennifer N. Sims**[1,2], **John Clohessy**[7], **Ann M. Dvorak**[2], **Tracey Sciuto**[2], **Manoj Bhasin**[5], **Joanne E. Murphy-Ullrich**[8], **Jack Lawler**[2], **S. Ananth Karumanchi**[3], and **Carmelo Nucera**[1,2,9]

[1]Laboratory of human thyroid cancers preclinical and translational research, Division of Experimental Pathology, Cancer Research Institute (CRI), Cancer Center, Department of Pathology, Beth Israel Deaconess Medical Center, Harvard Medical School, Boston, MA, USA

[2]Department of Pathology, Center for Vascular Biology Research (CVBR), Beth Israel Deaconess Medical Center, Harvard Medical School. Boston, MA, USA

[3]Department of Medicine, Center for Vascular Biology Research (CVBR), Beth Israel Deaconess Medical Center, Harvard Medical School. Boston, MA, USA

[4]Department of Pathology, Massachusetts General Hospital, Harvard Medical School, MA, Boston, USA

[5]Bioinformatic and Systems Biology Unit, Department of Medicine, Beth Israel Deaconess Medical Center, Harvard Medical School. Boston, MA, USA

[6]Longwood Small Animal Imaging Facility (LSAIF), Department of Radiology, Beth Israel Deaconess Medical Center, Harvard Medical School. Boston, MA, USA

[7]Division of Cancer Genetics, Department of Medicine, Beth Israel Deaconess Medical School, Harvard Medical School. Boston, MA, USA

**Corresponding:** Carmelo Nucera, M.D., Ph.D , Assistant Professor at Harvard Medical School, Laboratory of human thyroid cancers preclinical and translational research, Division of Experimental Pathology, Department of Pathology, Cancer Research Institute (CRI)/ Cancer Center, Beth Israel Deaconess Medical Center, Harvard Medical School, Broad Institute of MIT and Harvard, Cambridge, MA, USA, Office: RN270G, 99 Brookline Avenue, Boston, 02215, MA, cnucera@bidmc.harvard.edu, Phone: 617-667-5964, Fax: 617-667-3591.

Authors' Contributions

Study supervision: CN

Provision of materials for the study: CN

Writing of the manuscript: CN

Figures preparation: CN, AP

Development of methodology: AP (pericytes assays, secretome production, development of cell co-culture model, WB, drugs validations assays, and mouse data analyses), ZAA (apoptosis assays, gene transduction, mouse surgery assistance), DV (WB assays), PMS (IHC analyses), SB and MB (heatmap, networks/pathways analyses, and pericytes abundance), ASL (pericytes assays, secretome production, development of cell co-culture model, WB, drugs validations assays, ELISA, gene transduction, plasmids preparations, recombinant TGFβ1 assays, rescue experiments with active TGFβ1), JNS (wound healing assays), JC (oral gavage), AMD and TS (TEM), CN (supervision and design of all experiments).

Acquisition of data: AP, ASL, PMS, SB, ZAA, DV, SU, JNS, JC, TS, CN.

Analysis and interpretation of data: AP, ASL, PMS, SB, ZAA, DV, SU, JNS, JC, AMD, TS, MB, JEMU, JL, SAK, CN.

Review and/or revision of the manuscript: AP, ASL, PMS, SB, ZAA, DV, SU, JNS, JC, AMD, TS MB, JEMU, JL, SAK, CN.

Conflicts of interests

Authors have not conflicts to disclose for this manuscript.

[8]Departments of Pathology, Cell Developmental and Integrative Biology, and Ophthalmology, University of Alabama at Birmingham, Birmingham, AL, USA

[9]Broad Institute of MIT and Harvard, Cambridge, MA, USA

[#] These authors contributed equally to this work.

## Abstract

**Purpose:** The $BRAF^{V600E}$ oncogene modulates the papillary thyroid carcinoma (PTC) microenvironment, in which pericytes are critical regulators of tyrosine-kinase (TK)-dependent signaling pathways. Although $BRAF^{V600E}$ and TK inhibitors are available, their efficacy as bimodal therapeutic agents in $BRAF^{V600E}$-PTC is still unknown.

**Experimental Design:** We assessed the effects of vemurafenib ($BRAF^{V600E}$ inhibitor) and sorafenib (TKI) as single agents or in combination in $BRAF^{WT/V600E}$-PTC and $BRAF^{WT/WT}$ cells using cell-autonomous, pericyte co-culture, and an orthotopic mouse model. We also used $BRAF^{WT/V600E}$-PTC and $BRAF^{WT/WT}$-PTC clinical samples to identify differentially expressed genes fundamental to tumor microenvironment.

**Results:** Combined therapy blocks tumor cell proliferation, increases cell death, and decreases motility via $BRAF^{V600E}$ inhibition in thyroid tumor cells *in vitro*. Vemurafenib produces cytostatic effects in orthotopic tumors, whereas combined therapy (likely reflecting sorafenib activity) generates biological fluctuations with tumor inhibition alternating with tumor growth. We demonstrate that pericytes secrete TSP-1 and TGFβ1, and induce the rebound of pERK1/2, pAKT and pSMAD3 levels to overcome the inhibitory effects of the targeted therapy in PTC cells. This leads to increased $BRAF^{V600E}$-PTC cell survival and cell death refractoriness. We find that $BRAF^{WT/V600E}$-PTC clinical samples are enriched in pericytes, and TSP1 and TGFβ1 expression evoke gene-regulatory networks and pathways in the microenvironment essential for $BRAF^{WT/V600E}$-PTC cell survival. Critically, antagonism of the TSP-1/TGFβ1 axis reduces tumor cell growth and overcomes drug resistance.

**Conclusions:** Pericytes shield $BRAF^{V600E}$-PTC cells from targeted therapy via TSP-1 and TGFβ1, suggesting this axis as a new therapeutic target for overcoming resistance to $BRAF^{V600E}$ and TK inhibitors.

## Introduction

The Surveillance, Epidemiology, and End Results (SEER) cancer registry reveals that advanced-stage papillary thyroid cancer (PTC) is less tractable to therapy than localized PTC, as implied by increasing mortality rates [1]. $BRAF^{V600E}$ is a potent regulator of the MAPK (e.g. ERK1/2) pathway which is highly mutated in human cancers, and has been identified as a crucial and common oncogene in PTC. This mutation is associated with loss of radioiodine avidity, higher rates of recurrence and metastases, poorer prognosis, and lower survival rates [2] [3] [4]. Thus effective treatment of advanced PTC through $BRAF^{V600E}$ would meet an urgent clinical need.

Vemurafenib is the first FDA-approved $BRAF^{V600E}$ inhibitor for the treatment of $BRAF^{V600E}$-positive metastatic melanoma [5]. Vemurafenib binds to the ATP binding

cassette of mutated $BRAF^{V600E}$ and inhibits its pathway through ERK1/2. It has been used against metastatic $BRAF^{V600E}$-PTC that is refractory to radioiodine, but response has been variable and relapse is common [6]. Numerous mechanisms can promote resistance through bypass of pharmacologic $BRAF^{V600E}$ inhibition, which enables rebound of ERK1/2 [7, 8]. Another mechanism of resistance involves up-regulation of pro-angiogenic molecules such as the tyrosine kinases (TKs) in the microenvironment [9]. $BRAF^{V600E}$-PTC growth is influenced by the tumor microenvironment, which is in turn altered by the tumor itself, leading to abnormal extracellular matrix (ECM) deposition and activation of angiogenic pathways [10] [11]. Many of the processes involved in thyroid tumor growth and metastasis are mediated by signaling molecules downstream of activated TKs.

Another FDA-approved drug, sorafenib, inhibits both TKs and BRAF intracellular signaling. Sorafenib targets RET (including RET/PTC) to inhibit pro-angiogenic pathways such as VEGFR2 and PDGFRB [12], and is currently used to treat hepatocellular carcinoma, advanced renal carcinoma, and metastatic thyroid carcinoma [13]. However, resistance to sorafenib can develop in the first line setting in thyroid carcinoma patients [12, 14, 15], and $BRAF^{V600E}$ may impact treatment duration and promote resistance mechanisms to TK inhibitors.

Angiogenic factors confer survival advantages and are overexpressed in both tumor cells and blood vessels in PTC [16]. The angiogenic microenvironment includes pericytes, which are heterogeneous stromal cell populations that are fundamental to vessel stabilization and maturation and express a range of angiogenic factors (e.g. PDGFRB, VEGF, etc.) [17]. Pericytes regulate paracrine communications between tumor cells and microvascular endothelial cells in the thyroid gland [18] and human tumors [17]. In the tumor vasculature, pericytes protect endothelial cells from anti-angiogenic therapies, and may be players in resistance to vascular and microenvironment targeting drugs. They likewise confer survival advantages to endothelial cells through the secretion of pro-angiogenic factors [19]. However, pericyte depletion using genetic methods has led to more metastasis and enhanced epithelial-to-mesenchymal transition (EMT) in breast cancer models [20].

Thrombospondin-1 (TSP-1; THBS1 gene) is produced by tumor and stromal cell types and plays a fundamental role in regulating the angiogenic microenvironment as well as cell proliferation, adhesion, migration and invasion, and angiogenesis [21]. Its functional domains are crucial for cell-cell or cell-ECM interactions. It is enriched in the thyroid carcinoma microenvironment and plays an important role in tumor aggressiveness [22]. TSP-1 is also a key regulator of latent TGFβ activation, the conversion of latent TGFβ to its biologically active form in certain diseases [23]. TGFβ is an early tumor suppressor that is also a player in the metastatic switch of tumors, and promotes EMT and metastasis [24]. TGFβ-induced SMAD phosphorylation and EMT induction required MAPK pathway activation in murine thyrocytes derived from $BRAF^{V600E}$-mice, indicating that tumor initiation by $BRAF^{V600E}$ predisposes murine thyroid cells to TGFβ-induced EMT, through a MAPK-dependent process [25].

The inefficacy of single agent $BRAF^{V600E}$ or TKs inhibitors, and the eventual resistance to these agents, even in combination, highlight the need for a better understanding of the tumor

microenvironment, including the cross talk between pericytes and tumor cells. Therefore, in this study we have analyzed the effects of combined vemurafenib plus sorafenib therapy in $BRAF^{V600E}$ PTC patient-derived cells using cell cultures and *in vivo* models. Our results demonstrate that pericyte-derived secretomes increase pERK1/2, pAKT, and pSMAD3 levels in thyroid tumor cells to overcome the inhibitory effects of vermurafenib and sorafenib either alone or in combination. Pericyte-derived factors also increased survival of $BRAF^{V600E}$-tumor cells and refractoriness to tumor cell death. We demonstrate that pericytes are a source of both TSP-1 and TGFβ, and that antagonism of TSP1-dependent activation of latent TGFβ1 overcomes resistance to $BRAF^{V600E}$ inhibitors or TKI. Together, these data provide evidence. Thus, pericytes elicit resistance to vemurafenib and sorafenib therapy via the TSP-1/TGFβ1 axis, suggesting this axis as a promising new target in overcoming therapy resistance.

## Materials and Methods

### Cell cultures

We used authenticated (STR and DNA sequencing for KTC1; DNA sequencing and RT-PCR for TPC1) KTC1 ($BRAF^{WT/V600E}$) and TPC1 ($BRAF^{WT/WT}$) human thyroid carcinoma cell lines, and human pericytes ($BRAF^{WT/WT}$) were obtained from Promo Cell (Germany) [18]. The use of these cell lines was approved from the committee on microbiologal safety (COMS, Beth Israel Deaconess Medical Center (BIDMC), Boston, MA, USA). KTC1 is a spontaneously immortalized human thyroid carcinoma cell line which harbors $BRAF^{WT/V600E}$ mutation. It was established from the metastatic pleural effusion from recurrent and radioiodine (RAI) refractory PTC in a 60-year-old male patient [26] by Dr. J. Kurebayashi (Department of Breast and Thyroid Surgery Kawasaki Medical School Kurashiki, Japan) and provided by Dr. Rebecca E. Schweppe (University of Colorado, USA).

### Drug treatments

For our *in vitro* assays, we used 10 mM vemurafenib (PLX4032, RG7204, Cat#S1267) (Selleckchem, USA) dissolved in 100% dimethyl sulfoxide (DMSO, vehicle). Sorafenib tosylate (Cat#S1040, Selleckchem, USA), a multikinase inhibitor, was dissolved in 100% DMSO (Sigma, USA) according to manufacturer instructions to produce 10 mM stock solution. Intermediate doses of vemurafenib or sorafenib were prepared in 100% DMSO and diluted in 0.2% fetal bovine serum (FBS) DMEM to achieve desired final concentrations, maintaining a constant final concentration at 2% DMSO for optimal solubility (see Supplementary Methods). Synergy, sub-additive or additive activity for the combined treatments of vemurafenib plus sorafenib were estimated using GeoGebra Classic and applying Loewe test method according to Tallarida [27] to assess drug synergy and antagonism. Cells were treated for 48 hours in the presence of 0.2% FBS DMEM at final 2% DMSO with: 1, 2.5, 5 or 10 μM of either vemurafenib or sorafenib; or combined therapy with vemurafenib plus sorafenib combining all above doses. Vehicle was used as untreated control (2% DMSO diluted in 0.2% FBS DMEM). Before adding treatments, cells were washed with PBS from 10% FBS DMEM. Quantitative analysis was performed by crystal

violet assays (see Supplementary Methods) of adherent cells (magnification: 10×). Vehicle (control) was 2% DMSO diluted in 0.2% FBS DMEM.

### SRI31277 peptide

Peptide SRI31277 [24] was synthesized by BioMatik USA and purity confirmed at Southern Research. We reconstituted the peptide in 0.2% FBS DMEM) to achieve the stock concentration of 2.6 mM. SRI31277 was diluted in 0.2% FBS DMEM in order to achieve final concentration of 1 μM, 2.5 μM, 5 μM, 10 μM, 25 μM, 50 μM, or 100 μM.

### Model of pericyte secretome

Pericytes were seeded at about 90% confluence in 6-well dishes in DMEM growth medium supplemented with 10% FBS. Forty-eight hrs following cell seeding, pericytes were treated for 5 hours with 10 μM vemurafenib, 2.5 μM sorafenib, combined therapy with 10 μM vemurafenib plus 2.5 μM sorafenib, or vehicle (2% DMSO) in the presence of 0.2% FBS DMEM growth medium. Following treatment, the 0.2% FBS DMEM cell growth medium enriched by cell-derived secreted protein factors was defined as secretome and was normalized to the same cell growth medium in order to subtract background; then, it was collected and separated from dead cell debris by short spin. We collected an aliquot of secretome volume for ELISA analysis. Additionally, the remaining volume of all four secretomes was used to treat $BRAF^{WT/V600E}$-KTC1 and $BRAF^{WT/WT}$-TPC1 for 5 hours. At the same time another condition included $BRAF^{WT/V600E}$-KTC1 and $BRAF^{WT/WT}$-TPC1 cells (both cell lines were seeded at 90% confluence in the presence of 10% FBS DMEM growth medium the day prior to treatments) directly treated (without pericyte secretome) for 5 hours with 10 μM vemurafenib, 2.5 μM sorafenib, combined therapy with 10 μM vemurafenib plus 2.5 μM sorafenib, or vehicle (2% DMSO) in the presence of 0.2% FBS DMEM growth medium. Also, after secretome collection, adherent pericytes were lysed for protein extraction in order to perform Western blotting assays. After treatment of the $BRAF^{WT/V600E}$-KTC1 and $BRAF^{WT/WT}$-TPC1 thyroid tumor cells, we collected an aliquot of secretome volume for ELISA analysis (Suppl. Materials and Methods). Then we lysed the adherent thyroid tumor cells for protein extraction in order to perform Western blotting assays.

### Model of cell co-culture

mCherry-KTC1 and pericytes were seeded at 150,000 cells (1:1) per well in 6-wells dishes or 30,000 cells per well in 24-wells dishes. Forty-eight hrs following cell seeding, cells were treated for 48 hours with 10 μM vemurafenib, 2.5 μM sorafenib, combined therapy with 10 μM vemurafenib plus 2.5 μM sorafenib, or vehicle (2% DMSO) in the presence of 0.2% FBS DMEM growth medium. After 48 hours, the 0.2% FBS DMEM cell growth medium enriched by cell-derived secreted protein factors was defined as secretome and was normalized to the same cell growth medium in order to subtract background; then, it was collected for ELISA analysis (Suppl. Materials and Methods) and separated from dead cell debris by short spin. Adherent cells were fixed with 10% formalin for 20 minutes at room temperature. Cells were then washed with PBS. Cells were stained with 5 μM Hoechst 33342 (Nexcelom, USA) diluted in PBS for 15 minutes. Total number of cells (cell growth)/

well was analyzed by Celigo image cytometer (Nexcelom, USA). Data were plotted as matrix of cell count using both GraphPad Prism 6 and excel software.

### Western blotting

Cells were grown in 10-cm dishes in 10% FBS DMEM. They were treated with vehicle (DMSO), vemurafenib, sorafenib or combined vemurafenib plus sorafenib therapy in the presence of 0.2% FBS DMEM when reached about 90–100% confluence. Western blotting assays were performed according to standard procedure [11]. The intensity of each protein band was normalized to housekeeping protein band (tubulin or actin) and quantified by densitometry analysis (ImageJ software, USA)

### Orthotopic mouse model

All animal work was approved and done in accordance with federal, local, and institutional guidelines (IACUC) at the BIDMC (Boston, MA, USA). Human metastatic KTC1 tumor-derived cells harboring the heterozygous $BRAF^{V600E}$ mutation and engineered to express luciferase were cultured in 10-cm dishes and grown in DMEM medium supplemented with 10% FBS, penicillin, streptomycin, and amphotericin at 37°C with 5% $CO_2$ atmosphere. Prior to implantation, cells were trypsinized, gently centrifuged, and suspended in serum-free DMEM growth medium to achieve a cell suspension concentration ranged between $3.5\times10^6$ and $5\times10^6$ cells/10 μL. The cells were kept on ice until implantation. KTC1 cells were orthotopically injected in the right thyroid of 9-week-old male NSG mice (strain name: NOD.Cg-$Prkdc^{scid}$ $Il2rg^{tm1Wjl}$/SzJ; stock number: 005557) (n=5 per group) according to our previous experimental procedures [22]. Mice were randomly divided into four groups of 5 for the purpose of establishing a timeline of tumor cell growth and response to therapy with vemurafenib, sorafenib, combined therapy (vemurafenib plus sorafenib), or vehicle. Treatments were started 6 weeks after KTC1 tumor cells implantation and performed for 5 weeks.

### Vemurafenib and sorafenib preparation for mouse treatment

For *in vivo* studies, drug suspensions were prepared for vemurafenib (10 mg/ml in 2% hydroxypropylcellulose) and sorafenib (3.75 mg/mL according to Fendrich et al. [28]). Freshly prepared drug suspensions were stored at 4°C and used within 48 hours. Mice were dosed once daily with vehicle alone (control), vemurafenib (100 mg/kg), sorafenib (30 mg/kg), or combination of vemurafenib and sorafenib as indicated by oral gavage using a 22G needle.

### Differential gene expression, regulatory networks, pathways analysis, and pericytes abundance score in PTC clinical samples

In order to determine the association of a select set of 23 genes linked to extracellular matrix functions, pericyte functions, angiogenesis, cell growth, adhesion/migration/invasion, and metastasis pathways with BRAF mutational status, we performed analysis on the genes PTC TCGA data. We downloaded RNA-seq data of PTC from TCGA to analyze 23 genes differentially expressed using 211 $BRAF^{WT/V600E}$-PTC, 23 PTC harboring $BRAF^{WT/V600E}$ and hTERT mutations, and 256 $BRAF^{WT/WT}$-PTC samples. After performing analysis on

the 23 selected genes, we considered only those with raw p-values <0.05 and fold-change (FC) ≥1.2 or ≤−1.2 as significantly associated with BRAF mutational status. Network analysis was also performed. More details are reported in the Supplementary Methods. Pericyte abundance analysis was assessed by the ssGSEA algorithm using RNAseq expression data from NT and PTC TCGA samples. SSGSEA calculates separate enrichment scores for each pairing of a sample and gene set; each enrichment score represents the degree to which the genes in a particular set are coordinately up-regulated or down-regulated. We specified the positive signature for pericytes based on the expression of NG2, PDGFRB, αSMA, and CD90 genes. To identify samples enriched with pericytes, we used the genes PECAM1, LYVE1 and CD34 as negative signature. Based on score differences, we ranked samples from the highest enrichment of pericyte signature to the least enrichment.

### Statistical analysis

Statistical analysis was carried out using GraphPad Prism 6 software, Microsoft Excel, and GeoGebra Classic statistical tools. Chi-square test, T-student, Mann-Whitney test, one-way analysis of variance (ANOVA) for multiple comparisons tests, and Pearson correlation analysis were used. Data are reported as the averaged value, and error bars represent the standard deviation of the average for each group. Results with p values below 0.05 were considered statistically significant.

We also used virus transduction assays (for gene overexpression or knockdown); gene regulatory networks/pathway analyses; and TEM (for more details, see the Supplementary Methods).

## Results

### Anti-BRAF$^{V600E}$ (vemurafenib) and anti-TKs (sorafenib) combined therapy blocks cell proliferation, increases cell death, and decreases motility in PTC cells

As a first step toward suppressing PTC cell survival, we assessed anti-BRAF$^{V600E}$ (vemurafenib) and anti-multi-TK (sorafenib) combined therapy in heterozygous BRAF$^{WT/V600E}$ (KTC1) or BRAF$^{WT}$ (TPC1) tumor cells derived from invasive PTC (Fig. 1A). We have previously characterized the PTC microenvironment, which has pericytes [11], crucial components of the vasculature known to express TKs (e.g. PDGFRB), as well as other markers such as NG2 and αSMA [17]. Our results confirmed these findings (Fig. 1B), and human pericytes were also negative for mesenchymal and endothelial cell markers (Fig. 1B). Furthermore, transmission electron microscopy (TEM) revealed that human well-differentiated thyroid carcinoma tissue were characterized by endothelial cells and pericytes with a large nucleus and little cytoplasm as compared to the normal thyroid (NT) tissue (Fig. 1C). Pericytes may impact resistance in cancer by regulating TK-dependent angiogenic signaling pathways. We therefore analyzed the expression of two major TKs (PDGFRB and VEGFR2) in PTC-derived cells and human pericytes (Fig. 1D). Pericytes showed 3.7-fold and 5.1-fold changes in phospho(p)-PDGFRB-Y751 levels upon PDGFB treatment, and 1.1-fold and 1.38-fold changes in pVEGFR2-Y1059 levels upon VEGFA treatment when compared to KTC1 and TPC1 cells, respectively (Fig. 1D). PDGFB and VEGFA stimulated phosphorylation of PDGFRB and VEGFR2 in pericytes and BRAF$^{WT/V600E}$-PTC, but not in

$BRAF^{WT/WT}$-PTC, which showed low levels of these receptors (Fig. 1D). PDGFB stimulated VEGFR2 phosphorylation more than VEGFA did, possibly due to potential PDGFRB/VEGFR2 heterodimers; however, further studies are needed to define this phenomenon. To determine whether simultaneous inhibition of $BRAF^{V600E}$ and TKs was effective against tumor cells, we combined vemurafenib and sorafenib. Previous studies had identified the dose-response curve for vemurafenib (IC50, 50% maximal inhibitory concentration) in thyroid cancer cells [11]; to assess the most effective doses of combined vemurafenib plus sorafenib, we treated tumor cells for 48 hours with seven different drug dose combinations (Suppl. Fig.1). We used isobolographic analysis (Fig. 1E-F) to assess synergy or additivity. Our results showed that 10 μM vemurafenib plus 2.5 μM sorafenib had the highest therapeutic efficacy (synergistic effect) against $BRAF^{WT/V600E}$-PTC cells (Fig. 1E), but was sub-additive in $BRAF^{WT/WT}$-PTC cells (Fig. 1F) and pericytes (Suppl. Fig.2A). Specifically, the targeted therapy achieved a significantly lower viability (31%, 46%, and 49% by vemurafenib, sorafenib and combined therapy, respectively) in $BRAF^{WT/V600E}$-PTC cells than in pericytes (Suppl. Fig.2B). Similarly, combined therapy significantly decreased $BRAF^{WT/V600E}$-KTC1 cell viability compared to vehicle (60% decrease), vemurafenib (31% decrease), or sorafenib (20% decrease) (Suppl. Fig.1). In $BRAF^{WT/WT}$-TPC1 cells, combination therapy yielded a 23% decrease in cell viability compared to vehicle, 18% decrease compared to vemurafenib, and a 52% decrease compared to sorafenib (Suppl. Fig. 3). We also found significant induction of cell death in PTC-derived cells when we used combined therapy, as shown by cell death analysis (Fig. 1G). Combined therapy was significantly more effective than vehicle (21-fold increase), vemurafenib (7.3-fold increase), or sorafenib (10.8-fold increase) in inducing death in $BRAF^{WT/V600E}$-KTC1 cells (Fig. 1G). Also, vemurafenib (2.2-fold change increase) or combined therapy (2.1-fold change increase) induced significantly higher rate of cell death in $BRAF^{WT/V600E}$-KTC1 than $BRAF^{WT/WT}$-TPC1 cells, indicating the higher specificity of vemurafenib in targeting $BRAF^{WT/V600E}$ PTC cells vs. $BRAF^{WT/WT}$ PTC cells. In contrast, sorafenib was more effective on $BRAF^{WT/WT}$-TPC1 cells compared to $BRAF^{WT/V600E}$-KTC1 (0.51-fold change).

Furthermore, analysis of cell proliferation by BrdU (5-bromo-2-deoxyuridine) assay showed that targeting $BRAF^{V600E}$ by vemurafenib and sorafenib significantly inhibited DNA synthesis of PTC cells compared to vehicle or single agents. This effect was likely driven by combined therapy in $BRAF^{WT/V600E}$-KTC1 cells, but by sorafenib alone in $BRAF^{WT/WT}$-TPC1 cells (Fig. 1H-I). Significantly, high doses of vemurafenib were also required to inhibit melanoma cell viability [29]. Since $BRAF^{V600E}$ is a strong regulator of tumor cell migration [30], we applied a monolayer wound-healing (cell motility) assay to study the effects of cell migration during treatment (Fig. 1J-K). We measured the initial wound at baseline (time zero), treated the cells with vehicle, vemurafenib, sorafenib, or a combination of the two for 7 hours (a time point prior to any observed effects on cell proliferation), and then quantified healing area at 7 hrs vs. baseline in each condition (Fig. 1J-K). Importantly, $BRAF^{WT/V600E}$-KTC1 cells displayed a significant decrease in cell motility upon combination treatment as compared to vehicle at 7 hrs (Fig. 1J-K). In addition, vemurafenib treatment caused a decrease in cell motility compared to vehicle, while sorafenib did not (Fig. 1J-K). In summary, combined therapy blocked tumor cell proliferation, increased cell

death, and decreased motility in $BRAF^{WT/V600E}$-PTC cells, likely via $BRAF^{V600E}$ inhibition.

### Effects *in vivo* on tumor growth by targeted therapy in an orthotopic mouse model of human $BRAF^{WT/V600E}$-PTC.

We have developed the first interventional pre-clinical mouse trial of vemurafenib therapy in $BRAF^{WT/V600E}$-PTC patient-derived cells (Fig. 2A). Immunocompromised mice were orthotopically implanted with human KTC1 cells derived from recurrent $BRAF^{V600E}$-positive PTC, and engineered to express luciferase (Fig. 2B). Orthotopic tumors developed in all mice and were analyzed 6 weeks after injection as baseline (Fig. 2B). Mice were then randomized for treatment with vehicle, vemurafenib, sorafenib, or combined therapy with vemurafenib plus sorafenib. All tumors in the vehicle-treated mice exhibited a 3-fold increase in growth over baseline at week 5 (Fig. 2C). The vemurafenib dosage was similar to that of other studies [31]; here we found that only vemurafenib resulted in consistent reduction in tumor growth, likely due to cytostatic effects, with 61% significant reduction in tumor growth at week 4 and 48% reduction at week 5 as compared to vehicle-treated mice (Fig. 2B-C). Therapeutic response to sorafenib was fluctuant and resulted in a smaller reduction (23%) in tumor growth at week 4 and increased reduction (59%) at week 5 as compared to vehicle (Fig. 2B-C). Combined therapy followed the pattern of sorafenib activity and yielded a 5.1-fold increase (36%) in tumor growth at week 4 vs. vehicle, while a reduction (43%) in tumor growth occurred at week 5 vs. vehicle (Fig. 2B-C). We observed no apparent toxic side effects upon either single agent treatment or combined therapy. Since inhibition of $BRAF^{V600E}$ may redifferentiate thyroid tumor cells [32], we analyzed this phenomenon by microSPECT/CT imaging. Vemurafenib-treated mice at 5 weeks post-treatment showed >2-fold increase in $^{99m}Tc$ uptake, suggesting that targeting $BRAF^{V600E}$ could block not only tumor growth but also induce thyroid tumor re-differentiation more substantially than sorafenib (Fig. 2D-E).

### Pericyte secretome via the TSP-1/TGFβ1 axis evokes resistance to targeted therapy in $BRAF^{WT/V600E}$-PTC cells.

We have hypothesized that pericytes, which are fundamental to vessel maturation [33], are also fundamental to thyroid tumor cell viability, and limit the efficacy of $BRAF^{V600E}$ inhibitors and TKI. To test this hypothesis, we developed an experimental model using secretome derived from human pericytes treated for 5 hrs with either vehicle, vemurafenib, sorafenib, or combined therapy. Pericytes were grown in medium with low concentration of FBS (i.e. 0.2%) during treatment. The 0.2% FBS cell growth medium enriched by pericyte-derived secreted factors within 5 hrs of drug or vehicle treatment was defined as the secretome and was normalized to the same cell growth medium in order to subtract background. A multiplex ELISA assay (Suppl. Materials and Methods) including the most important cytokines and angiogenic factors showed no changes in secretion levels upon drug treatment (Suppl.Fig.4). Intracellular TSP-1 protein expression in pericytes was up-regulated within 5 hours of drug treatments (2.9-fold change with vemurafenib, 1.6-fold change with sorafenib and 1.7-fold change with combined therapy vs. vehicle) (Fig. 3A). In contrast, levels of secreted TSP-1 either fell or remained unchanged after treatment (12.1% decrease with vemurafenib, unchanged with sorafenib, and 15.3% decrease with combined therapy

vs. vehicle) (ELISA assay, Suppl. Materials and Methods) (Fig. 3B). Levels of secreted TGFβ1 likewise fell or remained unchanged after treatment (17.8% decrease with vemurafenib, unchanged with sorafenib, and 27.3% decrease with combined therapy vs. vehicle) (ELISA assay, Suppl. Materials and Methods) (Fig. 3B). TSP-1 is a mediator of TGFβ1 activation, which regulates many cell functions through SMAD, ERK1/2, AKT proteins [23, 24]. Moreover, we found that TKs levels were affected by the targeted therapy, i.e. PDGFRB phosphorylation levels were reduced upon drug treatment (43.6% decrease upon vemurafenib, 70.1% decrease upon sorafenib and 58.8% decrease upon combined therapy) vs. vehicle (Fig. 3A). pVEGFR2 protein decreased upon treatment with vemurafenib (20.0%) or sorafenib (22.4%), however, no substantial changes were observed upon combined therapy (Fig. 3A). Protein expression of pro-survival factors likewise fell in pericytes after drug treatment vs. vehicle treatment: **(i)** pAKT (94.5% decrease upon vemurafenib, 80.2% decrease upon sorafenib and 93.9% decrease upon combined therapy), **(ii)** pERK1/2 (15.7% decrease upon vemurafenib, 74.8% decrease upon sorafenib and 82.7% decrease upon combined therapy), and **(iii)** pSMAD3 (7.7% increase upon vemurafenib, 15.6% increase upon sorafenib, and 21.1% decrease upon combined therapy) (Fig. 3A).

It is known that $BRAF^{V600E}$ inhibitors such as vemurafenib selectively inhibit MAPK signaling (e.g. ERK1/2) in $BRAF^{WT/V600E}$ thyroid tumor cells [32, 34, 35]. To investigate the effects of pericytes on PTC-derived KTC1 or TPC1 cells, we treated these thyroid tumor cells for 5 hours with vemurafenib, sorafenib, or combined therapy in the presence or absence of the pericyte-derived conditioned medium (secretome) containing secreted TSP-1 and TGFβ1 (Fig. 3C). Importantly, pericytes and $BRAF^{WT/V600E}$-KTC1 cells were substantially responsive to treatment with exogenous recombinant human latent TGFβ1 protein (while response in $BRAF^{WT/WT}$-TPC1 cells was less robust), which upregulated pSMAD3 protein levels (Fig. 3D), suggesting the presence of endogenous regulators of latent TGFβ1. When we used a TSP-1 antagonist (i.e. SRI31277) derived from the LSKL sequence of latent TGFβ1 that blocks TSP1-mediated TGFβ1 activation [24] plus latent TGFβ1, we found pSMAD3 protein expression decreased 19% in pericytes vs. latent TGFβ1 treatment alone (Fig. 3D).

Since TSP-1 is also a key-player in aggressive anaplastic thyroid carcinoma (ATC) harboring $BRAF^{V600E}$ [22], we analyzed TSP-1 protein levels in aggressive PTC-derived cells. Interestingly, $BRAF^{WT/WT}$-TPC1 cells showed low intracellular TSP-1 protein levels (Suppl. Fig.5); also, secreted TSP-1 levels (as well as TKs pro-angiogenic factors, i.e. VEGFR2 or PDGFRB levels) were substantially lower (~20–50 folds) in $BRAF^{WT/WT}$-TPC1 cells compared to $BRAF^{WT/V600E}$-KTC1 cells across all treatments (Suppl. Fig.6A), suggesting expression of these factors might depend on the $BRAF^{V600E}$ pathway. Indeed, TSP-1 protein expression was down-regulated by direct drug treatments (without the presence of pericyte secretome) compared to vehicle in $BRAF^{WT/V600E}$-KTC1 cells, i.e. 15.5% by vemurafenib, 32.4% by sorafenib and 51.5% by combined therapy (Fig. 3E). Importantly, direct treatment by combined therapy more effectively down-regulated both TSP-1 (51.5% vs. vehicle), and the intracellular signaling effectors pERK1/2 (88% vs. vehicle), pAKT (58.8% vs. vehicle), and pSMAD3 (33.8% vs. vehicle), as well as TKs pVEGFR2 (38.2% vs. vehicle) and pPDGFRB (9.5% vs. vehicle) than single agents in

BRAF$^{WT/V600E}$-KTC1 cells (Fig. 3E). Vemurafenib treatment up-regulated pERK1/2, as expected, in BRAF$^{WT/WT}$-TPC1 cells (Suppl.Fig.5), likely due to paradoxical effects [36].

Since our mouse data suggested that kinase and angiogenesis inhibitors such as vemurafenib or sorafenib elicited cytostatic effects with differing levels of pharmacologic action (Fig. 2B-C), probably due to angiogenic microenvironment-mediated effects, we focused our attention on pericytes, denizens of the tumor microenvironment which are critical to vessel stabilization and angiogenic endothelial functions [33]. To understand the functional role of pericytes in paracrine communication with PTC cells, we assessed the ability of conditioned media (secretome) derived from pericytes to influence thyroid tumor cell intracellular signaling upon vehicle, vemurafenib, sorafenib, or combined treatment. As all pericyte secretome was collected within 5 hrs of treatment, it was unlikely to have been produced during deregulation of pathways related to cell death. Across all treatments, the presence of pericyte secretome as compared to no pericyte secretome (Fig. 3E) consistently and substantially increased levels of: **(i)** pERK1/2 (2.9-fold change with vehicle, 6.9-fold change with vemurafenib, 4.5-fold change with sorafenib, and 4.0-fold change with combined therapy); **(ii)** pAKT (1.7-fold change with vehicle, 11-fold change with vemurafenib, 3.5-fold change with sorafenib and 8.6-fold change with combined therapy); **(iii)** pSMAD3 (0.9-fold change with vehicle, 1.2-fold change with vemurafenib, 1.4-fold change with sorafenib and 2-fold change with combined therapy); **(iv)** TSP1 (1.6-fold change with vehicle, 1.4-fold change with vemurafenib, 1.9-fold change with sorafenib and 1.6-fold change with combined therapy); and **(v)** pVEGFR2 (1.02-fold change with vehicle, 1.9-fold change with vemurafenib, 1.6-fold change with sorafenib and 1.1-fold change with combined therapy) in BRAF$^{WT/V600E}$-KTC1 cells (Fig. 3E). As a result, pericytes provided significant growth advantages to BRAF$^{V600E}$-KTC1 cells, even when treated with vehicle (2.1-fold change compared to BRAF$^{WT/V600E}$-KTC1 tumor cells not co-cultured with pericytes) (Fig. 3F-G). These results may be linked to the ability of BRAF$^{V600E}$-KTC1 cells when stimulated by pericyte secretome (5 hrs) to significantly increase secretion of TSP-1 (150.2% with vehicle, 112.5% with vemurafenib, 104.9% with sorafenib, and 81.1% with combined therapy) and TGFβ1 (20.7% with vehicle, 83.9% with vemurafenib, 38.8% with sorafenib, and 47.2% with combined therapy) compared to the BRAF$^{WT/V600E}$-KTC1 cells without pericyte secretome (Fig. 3H). Pericyte secretome promoted a moderate rebound of pERK1/2 (but not when treated with vemurafenib), pAKT, and pSMAD3 in BRAF$^{WT/WT}$-TPC1 cells upon treatment with vehicle or drugs (Suppl.Fig.5).

Furthermore, we used one of the most efficient short hairpin RNA (shRNAs) [22] to knockdown TSP-1 in pericytes (Fig. 3I), down-regulating TSP-1 protein levels by more than 50%, and reducing secreted TSP-1 levels even more robustly upon drug treatment (Suppl.Fig.6B). Importantly, knockdown of TSP-1 (by shTSP-1) in pericytes substantially reduced the capability of the shTSP-1 pericyte secretome (compared to shGFP pericyte secretome, control) to trigger rebound of pERK1/2 (but not with combined therapy), pAKT, and pSMAD3 levels in BRAF$^{WT/V600E}$-KTC1 tumor cells (Fig. 3J). Also, secretion of TSP-1 decreased by 12.8% in BRAF$^{WT/V600E}$-KTC1 cells in the presence of the combined therapy-treated shTSP-1 pericyte secretome compared to shGFP secretome alone (Suppl.Fig. 6C). ShTSP-1 pericyte secretome did not have substantial additive effects in combination

with drug treatments in suppressing pERK1/2 (except with sorafenib, 29%) and pAKT levels, and exerted moderate effects in down-regulating pSMAD3 (22.5% with vemurafenib) in $BRAF^{WT/WT}$-TPC1 cells (Suppl.Fig.7), with no changes observed in the secreted levels of TSP-1 (only a moderate decrease with sorafenib, Suppl.Fig.6D), suggesting that $BRAF^{WT/WT}$-PTC cells may have a different TSP-1 regulatory pathway than $BRAF^{WT/V600E}$-PTC cells.

Overall, these results demonstrate that pericyte-derived secretome (e.g. TSP-1, TGFβ1) induces the rebound of pro-survival and pro-angiogenic factors and overcomes the inhibitory effects of targeted therapy in $BRAF^{WT/V600E}$-PTC cells, and ultimately contributes to an increase in $BRAF^{WT/V600E}$-thyroid tumor cell survival.

### Pharmacologic antagonism of TSP-1 by SRI31277 impairs TGFβ1-dependent signaling, reduces growth of $BRAF^{WT/V600E}$-PTC cells and overcomes resistance to targeted therapy.

The inhibition of TGFβ1 activation is a therapeutic strategy against cancer [24]. We used an antagonist (i.e. SRI31277) [24] that blocks TSP1-mediated TGFβ1 activation in the extracellular environment to determine the role of the TSP-1/TGFβ1 pathway in $BRAF^{WT/V600E}$-KTC1 cells using pSMAD3 protein expression. We assessed dose-response (IC50) for the SRI31277 peptide in $BRAF^{WT/V600E}$-KTC1 or $BRAF^{WT/WT}$-TPC1 cells, and in pericytes treated with a matrix of different doses (Suppl. Fig.8A-C). Our results showed that compared to vehicle, 10 μM SRI31277 provided a significant therapeutic effect against PTC cells and pericytes, reducing cell viability by 3.1-fold in $BRAF^{WT/V600E}$-KTC1, 4.1-fold in $BRAF^{WT/WT}$-TPC1, and 2.6-fold in pericytes (Suppl. Fig.8A-C). SRI31277 up-regulated pSMAD3 protein levels in pericytes within 5 hrs upon treatment with vehicle (37%) or vemurafenib (4.5%), and down-regulated its levels in the presence of sorafenib (4.7%) or combined therapy (27%) (Fig. 4A). Also, SRI31277 treatment substantially reduced both secreted TSP-1 (11%) and TGFβ1 (25.5%) in pericytes treated with combined therapy (Fig. 4B). Importantly, in $BRAF^{WT/V600E}$-KTC1 cells treated with pericyte secretome the pharmacologic antagonism of TSP-1 by SRI31277 treatment substantially down-regulated protein levels of pERK1/2 (23.4% with vehicle, 17.9% with vemurafenib, 37.7% with sorafenib, and 8.2% with combined therapy) and pSMAD3 (30.1% with vehicle, 27.4% with vemurafenib, 14.8% with sorafenib and 24.4% with combined therapy) (Fig. 4C, right panel). Intriguingly, we found that SRI31277 upregulated both pERK1/2 (100% with vehicle, 101% with vemurafenib, 24% with sorafenib, and 205% with combined therapy) and pSMAD3 (34.8% with vehicle, 21.1% with vemurafenib, 40.3% with sorafenib, and 25% with combined therapy) in the absence of pericyte secretome compared to vehicle in $BRAF^{WT/V600E}$-KTC1 cells (Fig. 4C, left panel). SRI31277 less robustly affected pERK1/2 and pSMAD3 levels in $BRAF^{WT/WT}$-TPC1 cells treated with pericyte secretome (Suppl.Fig. 9). Secreted levels of both TSP-1 (5% with vehicle, 58.6% with vemurafenib, 26.7% with sorafenib, and 52.3% with combined therapy) and TGFβ1 (17.1% with vehicle, 45.6% with vemurafenib, 27.9% with sorafenib, and 32% with combined therapy conditions) increased in $BRAF^{WT/V600E}$-KTC1 cells cultured with pericytes for 48 hrs compared to $BRAF^{WT/V600E}$-KTC1 cells in single culture (Fig. 4D). Importantly, the pharmacologic antagonism of TSP-1 by SRI31277 combined with $BRAF^{V600E}$ inhibition (vemurafenib) significantly reduced secretion of TSP-1 and TGFβ1 in $BRAF^{WT/V600E}$-KTC1 cells co-

cultured with pericytes compared to the KTC1 cell coculture without SRI31277 treatment (Fig. 4D). More importantly, the antagonism of TSP-1 by SRI31277 significantly overcame therapeutic resistance of $BRAF^{WT/V600E}$-KTC1 cell tumor growth inhibition to either vemurafenib (67.1% reduction vs. no SRI31277), sorafenib (63.1% reduction vs. no SRI31277), and combined therapy (66.5% reduction vs. no SRI31277) (Fig. 4E). We measured within 5 hrs of treatment the concentration of endogenous active TGFβ1 by ELISA in pericytes and KTC1 cells (Suppl. Materials and Methods). Active TGFβ1 represented a small fraction of the total TGFβ1 (reported in Fig. 3B and Fig. 3H). Specifically it was 21.8 pg/mL and 14.5 pg/mL with vehicle; 14.4 pg/mL and 6.6 pg/mL with vemurafenib, 22.6 pg/mL and 10.6 pg/mL with sorafenib; and 13.5 pg/mL and 6.8 pg/mL with combined therapy in $BRAF^{WT/V600E}$-KTC1 cells and pericytes, respectively. Finally, in order to overcome SRI31277 antagonism upon TGFβ1 activation by TSP-1, we treated $BRAF^{WT/V600E}$-KTC1 cells in pericytes coculture using the recombinant human active TGFβ1 (Fig. 4F). Importantly, cell stimulation by recombinant human active TGFβ1 protein significantly rescued $BRAF^{WT/V600E}$-KTC1 tumor cell growth in the coculture with pericytes within 48 hrs of treatment with SRI31277 plus sorafenib (1.34-fold, p=0.0075), and after treatment with SRI31277 plus combined therapy, TGFβ1 produced an even more robust rescue effect (8.7-fold, p=0.0044) (Fig. 4F). Stimulation with recombinant human active TGFβ1 was also effective in significantly enabling $BRAF^{WT/V600E}$-KTC1 tumor cell growth in the absence of SRI31277 treatment (1.4-, 3.1-, and 2.6-fold change upon vehicle, vemurafenib and combined therapy, respectively).

Taken together, these results indicate $BRAF^{WT/V600E}$-KTC1 cells elicit paracrine signals in synergy with pericytes, which contribute to tumor survival (Fig. 4E-F) via the TSP-1/TGFβ1 axis, and that pericytes trigger resistance to the targeted therapy.

### Effects of vemurafenib and sorafenib on the TSP-1/TGFβ1 axis in an orthotopic mouse model of human $BRAF^{WT/V600E}$-PTC.

Our *in vivo* mouse results (Fig. 2B-C) did not confirm the unique and synergistic effect of combined therapy with vemurafenib and sorafenib observed in our *in vitro* models (Fig. 1E-G), indicating the likely elicitation of drug resistance by the tumor microenvironment. Therefore, in order to assess the potential mechanisms of the apparent resistance to this targeted therapy, we have performed IHC on the orthotopic thyroid tumors. We found luciferase expression substantially decreased in orthotopic mouse tumors (Fig. 2B-C) after 5 weeks of treatment with either vemurafenib, sorafenib, or combined therapy (Fig. 5A). To corroborate these results, we analyzed the expression level of PAX8, a thyroid-specific marker, to identify $BRAF^{WT/V600E}$ human thyroid tumor cells [11], which matched the down-regulation of the luciferase marker in drug treated mice (Fig. 5A). We also used TUNEL (terminal deoxynucleotidyl transferase dUTP nick end labeling) to quantify cell death. Importantly, we found that vemurafenib moderately increased cell death in a subpopulation of tumor cells (Fig. 5A), whereas sorafenib treatment was less effective, as confirmed by *in vitro* results using the Annexin V/PI assay (Fig. 1G). Combined therapy with vemurafenib and sorafenib was found to induce cell death more effectively than single agents in a subpopulation of tumor cells (Fig. 5A), indicating that either $BRAF^{V600E}$ inhibitor (i.e. vemurafenib) or TKI (i.e. sorafenib) abrogates $BRAF^{WT/V600E}$-PTC through

complex mechanisms of action, ultimately resulting in cytostatic effects likely due to the presence of different clones with intrinsic primary resistance [34]. $BRAF^{WT/V600E}$ stimulates PTC cell proliferation (Fig. 1H), and affects the expression of TSP-1 and TGFβ1-dependent pSMAD3 and pERK1/2 (Fig. 3E, Fig. 4C), suggesting that this oncogene promotes thyroid tumor aggressiveness via the TSP-1/TGFβ1 axis. TSP-1 can inhibit VEGF-stimulated VEGFR2 phosphorylation in microvascular endothelial cells and block angiogenesis [37]. Since our *in vitro* data suggested a role for TSP-1 in the paracrine communication between $BRAF^{WT/V600E}$-PTC cells and pericytes, we assessed the expression of the TSP-1/TGFβ1 axis and pro-angiogenic factors *in vivo* in the angiogenic microenvironment of orthotopic $BRAF^{WT/V600E}$-PTC treated with vemurafenib, sorafenib, combined therapy, or vehicle (Fig. 5B). Combined therapy reflected the action of both vemurafenib and sorafenib in down-regulating cytosolic TSP-1 and TGFβ1 in tumor cells more than 50% compared to vehicle or single agents. Also, combined therapy reduced protein expression levels of pro-survival factors such as pAKT and tumor growth-related molecules such as pERK1/2. Critically, no inhibition (specifically by vemurafenib and combined therapy) of the TSP-1/TGFβ1 axis was observed in the vascular compartment, including endothelial cells and pericytes (Fig. 5B), suggesting that stromal vascular cells in the microenvironment can elicit drug resistance and provide advantages to PTC growth. With reduction of TSP-1 and TGFβ1 in tumor cells, we also found a substantial decrease (~2.5-fold change) in pSMAD3 expression involved in the TGFβ1 pathway in orthotopic thyroid tumor cells after treatment with vemurafenib or combined therapy, with no associated changes in the vascular/endothelial compartment (Fig. 5B). Additionally, vemurafenib substantially reduced pERK1/2 and pAKT levels in tumor cells but not in the vascular/endothelial compartment (Fig. 5B). In contrast, sorafenib treatment alone was ineffective in suppressing the expression of these intracellular signaling targets *in vivo* in both tumor and vascular cells (Fig. 5B). Vemurafenib (but not sorafenib) was ineffective at down-regulating markers of vascular density (e.g. CD31) (Fig. 5C), suggesting that vemurafenib specifically targets $BRAF^{V6000E}$-thyroid tumor cells but not $BRAF^{WT}$-stromal cells, and also that possibly sub-populations of stromal vascular cells elicit resistance to vemurafenib. Therefore, the tumor-associated vascular milieu may contribute to paracrine signaling and sustained $BRAF^{V6000E}$-thyroid tumor cell survival; indeed, we found no cell death effects from vemurafenib or combined therapy treatment in either $CD31^{+}$ (vascular endothelial cells), $NG2^{+}$, or $PDGFRB^{+}$ (markers of pericytes [17]) cells in the vascular compartment, including endothelial cells and pericytes (Fig. 5C). Interestingly, sorafenib produced a substantial reduction (~2-fold change) in the $\alpha SMA^{+}$ cell population (micro vessels) (Fig. 5C), and all drug treatments substantially decreased levels of pro-angiogenic factors VEGF and VEGFR2 in the tumor cells; in addition, vemurafenib reduced PDGFRB levels in the tumor cells. Only sorafenib and combined therapy (likely reflecting sorafenib activity) down-regulated PDGFB levels in cells of the vascular/endothelial compartment (Fig. 5C). Since $BRAF^{WT/V600E}$-PTC expresses high levels of adhesion molecules, which play important roles in the ECM of the tumor microenvironment [22] [10], we also performed trichrome staining of $BRAF^{WT/V600E}$-orthotopic PTC that revealed robust collagen deposition (Fig. 5D). Vemurafenib was associated with decreased collagen deposition (Fig. 5D), while sorafenib proved an ineffective mediator. When combined with vemurafenib, sorafenib limited its suppressive efficacy as well.

Collectively, these results indicate that combined therapy suppresses pro-angiogenic molecules and TSP-1/TGFβ1 expression in thyroid tumor cells but not robustly in the vascular compartment, including pericytes and endothelial cells. This heterogeneous therapeutic response may be linked to the presence of different subpopulations (lineage) of pericytes ($NG2^+$, $PDGFRB^+$, $\alpha SMA^+$ cells) in the tumor microenvironment which might trigger resistance to targeted therapy (i.e. $BRAF^{V600E}$ and TK inhibitors) (Fig. 3E). All information about antibodies used in this study is reported in Suppl. Table 1.

## The TSP-1/TGFβ1 axis regulates pathways fundamental for ECM angiogenic microenvironment and tumor growth in $BRAF^{WT/V600E}$-PTC compared to $BRAF^{WT/WT}$-PTC clinical samples.

TSP-1 mediates the interaction of tumor cells with the ECM [38], and plays a key role in progression when the $BRAF^{V600E}$ mutation is present [22]. TSP-1 also profoundly influences tumor cell proliferation, adhesion, and migration [22]. We therefore validated our TSP-1/TGFβ1 *in vitro* and mouse findings by assessing the functional interactions of TSP1-dependent regulatory gene networks in clinical samples of $BRAF^{WT/600E}$ or $BRAF^{WT/WT}$PTC. We used TCGA (The Cancer Genome Atlas samples [39] and applied the Linear model for RNA-seq data (Limma) for moderate T-statistics to identify genes fundamental to tumor growth and microenvironment functions that were differentially expressed in these two tumor groups. We analyzed 23 TCGA genes that are known to regulate ECM or pericyte function, angiogenesis, inflammation, immune response, cell viability and growth, cytoskeleton organization, adhesion/migration/invasion and metastasis. Nineteen out of 23 genes (82.6%) were significantly differentially expressed in $BRAF^{WT/600E}$ compared to $BRAF^{WT/WT}$ PTC; 10 out of 19 (52.7%) were up-regulated, and 9 out of 19 (47.3%) were down-regulated (Suppl. Table 2). The set of up-regulated genes included TSP-1 (THBS1) (Fig. 6A), which significantly increased (1.56-fold change) in $BRAF^{WT/600E}$-PTC (Suppl. Table 2). Furthermore, FN1, COL1A1, ITGA3, TGFβ, and THBS2, etc., which are crucial microenvironment-associated ECM components, were also up-regulated with significant fold-change ranging from 1.24 to 11.3. We found similar results when comparing PTC harboring both $BRAF^{WT/600E}$ and hTERT mutations (which has been reported in TCGA to co-occur in a very small number of PTC samples [39]) versus either $BRAF^{WT/V600E}$-PTC (Suppl. Tables 3, Suppl.Fig.10) or $BRAF^{WT/WT}$-PTC (Suppl. Tables 4, Suppl.Fig.11), indicating that $BRAF^{V600E}$ is important in the transcriptional regulation of TSP-1 and other genes with functions linked to the tumor microenvironment, including the vascular compartment and associated endothelial cells and pericytes. The significantly differentially expressed genes were used to build a TSP-1 gene regulatory network enrichment using the Cytoscape Genemania algorithm that also included gene co-expression results from TCGA. Each node identified genes and each edge represented functional interactions between genes. We found significant interactions between the up-regulated genes in $BRAF^{WT/V600E}$-PTC vs. $BRAF^{WT/WT}$-PTC samples. TSP-1 significantly interacted with all up-regulated genes, and more importantly was co-expressed with the TGFβ1 gene (Fig. 6B), suggesting the importance of TSP-1 in the direct regulation of TGFβ1 activation and pathways. We next carried out a TSP-1 pathways enrichment analysis (Fig. 6C), which identified significant pathways crucial for TGFβ signaling, metastasis, inflammation, immune modulation, tumor microenvironment-associated ECM remodeling

functions, tumor growth, and VEGF ligand-VEGF receptor interactions, etc. Importantly, many genes involved in these pathways are known to play roles in endothelial cell and pericyte functions in the vascular compartment. We found similar results when we compared PTC harboring both $BRAF^{WT/600E}$ and hTERT mutations vs. $BRAF^{WT/WT}$-PTC (Suppl.Fig. 12). Furthermore, we quantified pericyte abundance (Fig. 6D) using canonical markers such as αSMA, PDGFRB, NG2 [17], and CD90 (THY1) and the single sample Gene Set Enrichment Analysis (ssGSEA) algorithm applied to PTC TCGA data. From a set of 538 samples (59 NT and 479 PTC), we identified the 5% most pericyte-enriched (n=27, all PTC) and 5% least pericyte-enriched (n=27, 21 NT and 6 PTC) according to the PTC TCGA data (Fig. 6D). The remaining 90% of samples that included 38/59 NT or 446/479 PTC (185 $BRAF^{WT/V600E}$-PTC, 20 PTC with both $BRAF^{WT/V600E}$ and hTERT mutations, and 241 $BRAF^{WT/WT}$-PTC) ranked in the middle (mediocre) range (defined as 'average samples' with neither high nor low pericyte enrichment) of pericyte abundance scores (Fig. 6D). Specifically, NT samples were significantly overrepresented (3.5 folds, $p<0.001$) in the low pericytes-enriched group (21 out of 27, 77.7%) as compared to PTC samples (6/27, 22.2%). In contrast, 27 out of 33 PTC samples (81.8%) showed substantial enrichment (4.5-fold increase) in pericytes while only 6 out of 33 samples (18.1%) showed lower enrichment. Of the samples exhibiting a high abundance of pericytes (n=27), 16 (59.2%) were $BRAF^{WT/V600E}$-PTC ($p<0.001$, compared to NT), 3 (11.1%) were PTC with both $BRAF^{WT/V600E}$ and hTERT mutations, and 8 (29.6%) were $BRAF^{WT/WT}$-PTC, and none were NT. Of the samples with the least enrichment (n=27), 5 (18.5%) were $BRAF^{WT/V600E}$-PTC and 1 (3.7%) were $BRAF^{WT/WT}$-PTC, whereas the vast majority (n=21) were NT ($p<0.001$, compared to $BRAF^{WT/V600E}$-PTC with high abundance of pericytes). Therefore high pericyte enrichment aligned with $BRAF^{WT/V600E}$-PTC, and was 2-fold or 5.3-fold higher than levels observed in $BRAF^{WT/WT}$-PTC or PTC with both $BRAF^{WT/V600E}$ and hTERT samples, respectively (Fig. 6D). Importantly, intermediate risk of recurrence as assessed by the PTC TCGA clinical data base was associated with the 33 PTC samples as follows: 15/33 (45.4%) were $BRAF^{WT/V600E}$-PTC, 4/33 (12.1%) were $BRAF^{WT/WT}$-PTC, and 1/33 (3%) were PTC with $BRAF^{WT/V600E}$ and hTERT mutations. Importantly, among the $BRAF^{WT/V600E}$-PTC samples with intermediate risk of recurrence, 13/15 (86.6%) exhibited a high abundance of pericytes, whereas 2/15 (13.3) showed low pericyte enrichment. Also, Three out of 4 (75%) of $BRAF^{WT/WT}$-PTC samples with intermediate risk of recurrence showed high pericyte enrichment, and 1/4 (25%) showed low pericyte enrichment. No associations were found in PTC samples between BRAF mutational status, the low or high risk category, and pericytes abundance score. Overall, our data analysis indicated that pericytes population increased in $BRAF^{WT/V600E}$PTC than PTC with other genetic alterations, or even more robust than in NT samples (Fig. 6D). Collectively, our data indicate different activity by targeted therapy with vemurafenib or sorafenib on the regulation of angiogenesis and ECM molecules expression in the $BRAF^{WT/V600E}$-KTC1 orthotopic tumor cells and vascular/endothelial compartment (Fig. 6E). $BRAF^{WT/600E}$-PTC cells evoke paracrine regulatory networks to recruit pericytes, which ultimately sustain tumor cell survival. Overall, our findings reveal a new model of resistance to vemurafenib and sorafenib therapy in $BRAF^{WT/V600E}$-PTC via the TSP-1/TGFβ1 axis triggered by pericytes (Fig. 6F-G).

## Discussion

Although thyroid cancer mortality rates are lower relative to incidence rates, thyroid cancer mortality has nevertheless increased significantly since the late 1980s [1]. Patients diagnosed with thyroid cancer can be treated with radioactive iodine, but a subset of patients fails to respond to this treatment and suffer low survival rates [40], due to the $BRAF^{V600E}$ mutation. To date, most clinical trials for metastatic thyroid cancer have focused on single agents with low response rates; more effective treatment options for this disease are urgently needed. The prevalence and critical role of genetic mutations in cancer cells have led to targeted molecular therapy. Current therapies target $BRAF^{V600E}$, MEK, PI3K, TKs, etc. Since $BRAF^{V600E}$ is the most frequent oncogene implicated in PTC initiation [32] and aggressiveness [22], targeting this mutation holds great promise for future therapies. Small molecule kinase inhibitors allow for fewer side effects than traditional chemotherapy; however, most cancers are heterogeneous and have the capacity to develop resistance to targeted therapies [41]. Sorafenib was the first targeted therapy approved for patients with advanced differentiated thyroid carcinoma (DTC) [42]. It is an oral multi-kinase inhibitor that is used as first-line treatment for metastatic DTC. When tumors grow, they generate new blood vessels by angiogenesis to supply adequate nutrients [43]. Researchers have therefore focused on anti-angiogenic therapy, including disruption of new blood vessels, to suppress tumor growth. Sorafenib has been considered a possible angiogenesis disruptor [44]. Here we have shown, however, that thyroid tumor cells harboring the $BRAF^{V600E}$ mutation elicit resistance to sorafenib and limit its therapeutic efficacy.

Other systemic therapies have been used against DTC in the clinic; we chose to investigate vemurafenib, the first FDA-approved selective oral inhibitor of $BRAF^{V600E}$ [45]. Vemurafenib has been used in patients with metastatic and radioiodine refractory $BRAF^{V600E}$-PTC and continuously administered twice a day in cycles of 28 days [6]. This therapy showed anti-tumor activity with partial response in 10/26 patients (38.5%, best overall response). Four patients (15%) died after a median follow-up of 18.8 months. It is unclear whether the similarities of drug targets in DTC could lead to complete cross-resistance and whether sequential treatment would be efficacious. Previous studies revealed that treatment of $BRAF^{V600E}$-positive thyroid cancer cells with vemurafenib initially produced a therapeutic response, however, mechanisms of resistance were quickly elicited which led to cell death refractoriness [8] [35] [11] [34]. Also, studies on $BRAF^{V600E}$ human melanoma cells showed resistance to completely suppress ERK1/2 activation even with high doses of vemurafenib [46], similar to our results using the 10 μM dosage. Our study is the first to show data on combined inhibition of both $BRAF^{V600E}$ and tyrosine kinase as a potential targeted therapeutic option. Combined therapy with vemurafenib and sorafenib showed synergistic effects in $BRAF^{WT/V600E}$-PTC cells, whereas it was sub-additive in $BRAF^{WT/WT}$-PTC cells and pericytes. As a result, this combined inhibition was significantly more effective than vehicle or single agents in inducing higher rates of death in $BRAF^{WT/V600E}$-PTC than $BRAF^{WT/WT}$-PTC cells. However, our mouse data showed that vemurafenib produced cytostatic effects in orthotopic tumors, whereas combined therapy (likely reflecting sorafenib activity) generated biological fluctuations with tumor inhibition alternating with tumor growth. To understand this phenomenon, we subsequently analyzed

the microenvironments of orthotopic $BRAF^{WT/V600E}$-PTC, and found these tumors were enriched with heterogeneous populations of pericytes, in particular PDGFRB+, αSMA+, and NG2+. Many genetic alterations, including the $BRAF^{V600E}$ oncogene, confer a cell-autonomous fitness advantage to tumors by providing independence from growth factors or suppressing cell death responses. Additionally, tumor progression is affected by microenvironment-associated factors that cannot be overcome by adopting targeted therapies against only tumor cells *per se*. The combined vemurafenib plus sorafenib therapy showed synergy effects against $BRAF^{WT/V600E}$-PTC cells but not $BRAF^{WT/WT}$-PTC cells or pericytes, suggesting biological cooperation between $BRAF^{V600E}$ and TK pathways. This therapeutic synergy inhibited activation of ERK1/2, AKT, and TKs (e.g. VEGFR2, PDGFRB) to suppress tumor survival and motility.

The depletion of pericytes in transgenic mice under control of NG2 promoter inhibited breast tumor growth and defective tumor vasculature, but in one study was also found to increase metastasis [20]. In the context of $BRAF^{WT/600E}$-PTC, pericytes could elicit resistance driven by higher intracellular levels of TSP-1. Intracellular TSP-1 was found to behave differently in pericytes than in $BRAF^{WT/600E}$-PTC cells upon the administration of targeted therapy; i.e., pericytes treated with the targeted therapy up-regulated intracellular TSP-1, whereas $BRAF^{WT/600E}$-PTC cells down-regulated it. This might be due to the fact that thrombospondins, including TSP-1, are ER-resident effectors of adaptive ER stress [47], and can function inside the cell during stress, tissue damage, or active remodeling to augment ER function [47]. Here, we found that pericytes secreted TSP-1 and TGFβ1, and induced the rebound of pERK1/2, pAKT and pSMAD3 levels to overcome the inhibitory effects of the targeted therapy in $BRAF^{WT/600E}$-PTC cells. This led to increased $BRAF^{V600E}$-PTC cell survival and cell death refractoriness, indicating that accumulated intracellular TSP-1 might drive this effect. These intracellular signaling effectors were suppressed by direct treatment with vemurafenib or sorafenib, and more strongly by combined therapy, suggesting that microenvironment-associated pericytes represent one of the constraints for these targeted therapies. It has been reported that pericytes can communicate with tumor cells and endothelial cells by paracrine communication to ultimately elicit tumor cell survival [19]. Combined therapy against $BRAF^{WT/V600E}$-PTC cells alone strongly induced cell death and inhibited proliferation, but when these tumor cells were co-cultured with pericytes, they showed increased cell survival. More importantly, our *in vivo* findings showed that combined therapy effectively suppressed the expression of both TSP-1/TGFβ1 and TKs pathways in tumor cells but not in the vascular compartment. We can argue, therefore, that vascular microenvironment-derived TSP-1 is an important factor in drug resistance in PTC, which functions in a signaling network with intracellular TSP-1, TGFβ1/SMAD and TKs (i.e. VEGFR2, PDGFRB) for the regulation of tumor growth, as was confirmed in our PTC clinical sample data analysis. Importantly, specific sequences in the thrombospondin type 1 repeats (TSR) are critical for activating latent TGFβ1 through disruption of the LSKL sequence in the latency-associated peptide region of latent TGFβ1 within the mature domain, which re-conforms the latent complex to make it accessible to TGFβ signaling receptors [48]. Peptides of the LSKL sequence or related analogues such as SRI31277, antagonize TGFβ activation by preventing TSP-1 binding to the latent complex [24]. Like TSP-1, TGFβ1 plays an important role in tumorigenesis and

angiogenesis. TGFβ signaling can be pro-tumorigenic or tumor suppressive [49, 50]. TGFβ acts through membrane receptor kinases to activate SMAD transcription factors for many biological functions [51]. To assess the role of this pathway in PTC cells and pericytes, we used the SRI31277 peptide, which antagonizes TSP-1 activity on TGFβ1 activation. This peptide showed significant anti-tumor effects against multiple myeloma [24]. In our study, we analyzed the specificity of the TSP1-driven drug resistance mechanism promoted by pericytes in PTC cells through both an SRI31277-based pharmacologic approach and an shRNA strategy; together these showed that antagonism or knockdown of TSP-1, respectively, down-regulated TGFβ1 pathways in PTC cells when these cells were stimulated with pericyte secretome. Ultimately, this disruption of the TSP-1/TGFβ1 axis recovered the ability of the targeted therapy to inhibit $BRAF^{WT/V600E}$-PTC intracellular cell signaling, leading to significant decrease in tumor cell growth. Our data also indicated that pericyte populations expressing PDGFRB and NG2 were unchanged by any treatment in our orthotopic mouse model of human $BRAF^{WT/V600E}$-PTC, whereas pericytes expressing αSMA were substantially reduced upon administration of sorafenib alone, despite this treatment yielding no significant tumor growth reduction, which suggests that the αSMA+ cell subpopulation may be susceptible to induction of cell death by TK inhibitors (e.g. sorafenib). Recruitment of αSMA+ pericytes around teratocarcinoma vessels indicated vessel differentiation and higher tumor cell proliferation [52]. Our results therefore suggest that diverse pericyte subpopulations play multiple roles in the PTC microenvironment, as shown in other tumor models [17], and may destabilize vessels and promote/sustain $BRAF^{WT/V600E}$-PTC cell-to-ECM adhesion for survival, motility and ultimately vascular invasion. Further studies will be needed, however, to explore these possibilities, characterize pericyte subpopulations, and determine the level of activation of pericytes in thyroid carcinoma. In glioblastoma, a contact-dependent interaction with tumor cells switched on the tumor-promoter character of pericytes, inducing their participation in tumor progression [53]. Importantly, $BRAF^{WT/V600E}$-PTC samples showed higher pericyte enrichment than $BRAF^{WT/WT}$-PTC or NT samples, as well as a significant abundance of ECM molecules, which may be linked to the activation of regulatory gene networks and pathways fundamental for tumor growth, angio-invasion, and metastasis. Pericytes express and secrete ECM molecules that are important for cell survival, adhesion, and migration [18], and support processes important to the efficient alignment of endothelial cells required for maturation of capillary structures and delivery of nutrients. Ultimately this process might contribute to $BRAF^{WT/V600E}$-PTC cell survival, extra-thyroidal extension, angio-invasion, and metastasis. Since humans and mice have different oral drug bioavailability, physiology and metabolism, vemurafenib and sorafenib doses used in mice are not comparable to those appropriate to human patients. Vemurafenib was substantially more effective than sorafenib at inhibiting tumor growth *in vivo,* and caused both cytotoxic and cytostatic effects, as well as down-regulation of TSP-1, TGFβ1, SMAD3, ERK1/2 and AKT protein levels in tumor cells, but not in the vascular compartment, including endothelial cells and pericytes. Overall, our results indicate that the TSP-1/TGFβ1 axis is expressed and functional in the PTC microenvironment and might contribute to targeted therapy resistance. Our findings also revealed an abundance of collagen deposition, another key player in migration and angio-invasion, in the orthotopic tumors treated with either sorafenib or combined therapy, but not vemurafenib. Sorafenib primarily acted as an anti-angiogenic agent, suppressing VEGFR2

expression in the orthotopic tumor cells, and VEGF and PDGFB protein expression levels in the vascular compartment/endothelial; however, it was ineffective in blocking the likely expression of ECM molecules (e.g. collagen) in the thyroid tumor microenvironment, and maintained high protein levels of pERK1/2, pSMAD3 and pAKT. Ultimately, this effect substantially extended tumor survival compared to vemurafenib treatment, and negatively impacted the therapeutic efficacy of the combined treatment as well. Critically, it has been suggested that TSP-1 may regulate the expression of collagen in response to stress and tissue remodeling, independent of TGFβ1 activation [54]. One possibility is that ER stress response may lead to a lack of TSP-1 suppression and cause hyper-secretion of ECM molecules such as collagen and fibronectin. Furthermore, we found these ECM molecules transcriptionally up-regulated in $BRAF^{WT/V600E}$-PTC compared to $BRAF^{WT/WT}$-PTC clinical samples, indicating that the $BRAF^{V600E}$ oncogene deregulates ECM composition, and not only provides growth advantages to PTC cells but also promotes cell adhesion/migration, leading to intravascular invasion and metastasis (e.g. to the neck lymph node compartments), which is frequent in $BRAF^{WT/V600E}$-PTC.

Collectively, our results indicate that the action of the TSP-1/TGFβ1 axis enables drug resistance to $BRAF^{V600E}$ and TK inhibitors in $BRAF^{WT/V600E}$-PTC cells. Our study is limited by a lack of human samples from patients with metastatic $BRAF^{V600E}$-PTC treated with $BRAF^{V600E}$ inhibitors and TKI; however, our results are substantiated by our integrated cell cultures, cell co-cultures, and mouse model, as well as the use of TCGA clinical samples of PTC. We cannot exclude the possibility that this resistance mechanism is specific only to sorafenib. Further studies will be needed to assess $BRAF^{V600E}$ inhibitors in combination with other TK inhibitors such as lenvatinib. Also, since TGFβ1 is known to evoke active immune suppression, future research could assess the effects of pharmacologic antagonism of the TSP-1/TGFβ1 axis on the immune microenvironment of thyroid carcinomas.

**In summary**, our findings indicate that pericytes may be a double-edged sword in $BRAF^{WT/V600E}$-PTC therapy, and secrete soluble factors, such as TSP-1 and TGFβ1, that trigger resistance to $BRAF^{V600E}$ inhibitors and TKI in $BRAF^{WT/V600E}$-PTC. Pharmacologic antagonism of TSP-1 to block TGFβ1 activation may be crucial for the inhibition of tumorigenic effects by TGFβ1 pathway in $BRAF^{WT/V600E}$-PTC cells. This might represent a novel therapeutic strategy with translational applications in clinical trials against $BRAF^{WT/V600E}$-PTC resistant to targeted therapies. Finally, TSP-1 is a potential biomarker for assessing therapeutic response to $BRAF^{V600E}$ and TK inhibitors in patients with invasive $BRAF^{WT/V600E}$-PTC.

## Supplementary Material

Refer to Web version on PubMed Central for supplementary material.

## Acknowledgements

Carmelo Nucera (Principal Investigator, Human Thyroid Cancers Preclinical and Translational Research at the Beth Israel Deaconess Medical Center (BIDMC)/Harvard Medical School) was awarded grants by the National Cancer Institute/National Institutes of Health (1R21CA165039–01A1 and 1R01CA181183–01A1), the American Thyroid

Association (ATA) and ThyCa:Thyroid Cancer Survivors Association Inc. for Thyroid Cancer Research. Carmelo Nucera was also a recipient of the Guido Berlucchi “Young Investigator” research award 2013 (Brescia, Italy) and BIDMC/CAO Grants (Boston, MA). SRI31277 production and JEMU’s contributions were supported by NIH grant 1R01CA175012. We are grateful to Prof. Harold F. Dvorak and Miss Elizabeth McGonagle (BIDMC/HMS) for critical reading of our manuscript. We are grateful to Dr. Andrew L. Kung Dr. Andrew L. Kung (Memorial Sloan Kettering Cancer Center, NYC, USA) for kindly providing the FUW-Luc-mCherry-puro (luciferase/cherry) plasmid, and to Prof. Judy Lieberman and Dr. Minh T.N. Le (Children’s Hospital, Harvard Medical School, Boston, USA) for kindly providing packaging plasmids (psPAX2, pMD2-G, and RTR2). We also thank Miss Nicole Pandell for the technical support for the oral gavages in the mice.

## References

1. Lim H, et al., Trends in Thyroid Cancer Incidence and Mortality in the United States, 1974–2013. JAMA, 2017 317(13): p. 1338–1348. [PubMed: 28362912]
2. Xing M, et al., Association between BRAF V600E mutation and mortality in patients with papillary thyroid cancer. JAMA, 2013 309(14): p. 1493–501. [PubMed: 23571588]
3. Xing M, et al., Association between BRAF V600E mutation and recurrence of papillary thyroid cancer. J Clin Oncol, 2015 33(1): p. 42–50. [PubMed: 25332244]
4. Liu R, et al., Mortality Risk Stratification by Combining BRAF V600E and TERT Promoter Mutations in Papillary Thyroid Cancer: Genetic Duet of BRAF and TERT Promoter Mutations in Thyroid Cancer Mortality. JAMA Oncol, 2016.
5. Chapman PB, et al., Improved survival with vemurafenib in melanoma with BRAF V600E mutation. N Engl J Med, 2011 364(26): p. 2507–16. [PubMed: 21639808]
6. Brose MS, et al., Vemurafenib in patients with BRAF(V600E)-positive metastatic or unresectable papillary thyroid cancer refractory to radioactive iodine: a non-randomised, multicentre, open-label, phase 2 trial. Lancet Oncol, 2016 17(9): p. 1272–82. [PubMed: 27460442]
7. Nucera C, Evolution of resistance to thyroid cancer therapy. Aging (Albany NY), 2016 8(8): p. 1576–7. [PubMed: 27575377]
8. Montero-Conde C, et al., Relief of feedback inhibition of HER3 transcription by RAF and MEK inhibitors attenuates their antitumor effects in BRAF-mutant thyroid carcinomas. Cancer Discov, 2013 3(5): p. 520–33. [PubMed: 23365119]
9. Nazarian R, et al., Melanomas acquire resistance to B-RAF(V600E) inhibition by RTK or N-RAS upregulation. Nature, 2010 468(7326): p. 973–7. [PubMed: 21107323]
10. Nucera C, Lawler J, and Parangi S, BRAF(V600E) and microenvironment in thyroid cancer: a functional link to drive cancer progression. Cancer Res, 2011 71(7): p. 2417–22. [PubMed: 21447745]
11. Duquette M, et al., Metastasis-associated MCL1 and P16 copy number alterations dictate resistance to vemurafenib in a BRAFV600E patient-derived papillary thyroid carcinoma preclinical model. Oncotarget, 2015 6(40): p. 42445–67. [PubMed: 26636651]
12. Brose MS, et al., Sorafenib in radioactive iodine-refractory, locally advanced or metastatic differentiated thyroid cancer: a randomised, double-blind, phase 3 trial. Lancet, 2014 384(9940): p. 319–28. [PubMed: 24768112]
13. Pitoia F and Jerkovich F, Selective use of sorafenib in the treatment of thyroid cancer. Drug Des Devel Ther, 2016 10: p. 1119–31.
14. Kloos RT, et al., Phase II trial of sorafenib in metastatic thyroid cancer. J Clin Oncol, 2009 27(10): p. 1675–84. [PubMed: 19255327]
15. Sherman EJ, et al., Phase 2 study evaluating the combination of sorafenib and temsirolimus in the treatment of radioactive iodine-refractory thyroid cancer. Cancer, 2017.
16. Bunone G, et al., Expression of angiogenesis stimulators and inhibitors in human thyroid tumors and correlation with clinical pathological features. Am J Pathol, 1999 155(6): p. 1967–76. [PubMed: 10595926]
17. Song S, et al., PDGFRbeta+ perivascular progenitor cells in tumours regulate pericyte differentiation and vascular survival. Nat Cell Biol, 2005 7(9): p. 870–9. [PubMed: 16113679]
18. Sadow PM, et al., Role of BRAFV600E in the first preclinical model of multifocal infiltrating myopericytoma development and microenvironment. J Natl Cancer Inst, 2014 106(8).

19. Franco M, et al., Pericytes promote endothelial cell survival through induction of autocrine VEGF-A signaling and Bcl-w expression. Blood, 2011 118(10): p. 2906–17. [PubMed: 21778339]
20. Cooke VG, et al., Pericyte depletion results in hypoxia-associated epithelial-to-mesenchymal transition and metastasis mediated by met signaling pathway. Cancer Cell, 2012 21(1): p. 66–81. [PubMed: 22264789]
21. Yee KO, et al., Expression of the type-1 repeats of thrombospondin-1 inhibits tumor growth through activation of transforming growth factor-beta. Am J Pathol, 2004 165(2): p. 541–52. [PubMed: 15277228]
22. Nucera C, et al., B-Raf(V600E) and thrombospondin-1 promote thyroid cancer progression. Proc Natl Acad Sci U S A, 2010 107(23): p. 10649–54. [PubMed: 20498063]
23. Crawford SE, et al., Thrombospondin-1 is a major activator of TGF-beta1 in vivo. Cell, 1998 93(7): p. 1159–70. [PubMed: 9657149]
24. Lu A, et al., Inhibition of Transforming Growth Factor-beta Activation Diminishes Tumor Progression and Osteolytic Bone Disease in Mouse Models of Multiple Myeloma. Am J Pathol, 2016 186(3): p. 678–90. [PubMed: 26801735]
25. Knauf JA, et al., Progression of BRAF-induced thyroid cancer is associated with epithelial-mesenchymal transition requiring concomitant MAP kinase and TGFbeta signaling. Oncogene, 2011 30(28): p. 3153–62. [PubMed: 21383698]
26. Kurebayashi J, et al., All-trans-retinoic acid modulates expression levels of thyroglobulin and cytokines in a new human poorly differentiated papillary thyroid carcinoma cell line, KTC-1. J Clin Endocrinol Metab, 2000 85(8): p. 2889–96. [PubMed: 10946899]
27. Tallarida RJ, Quantitative methods for assessing drug synergism. Genes Cancer, 2011 2(11): p. 1003–8. [PubMed: 22737266]
28. Fendrich V, et al., Sorafenib inhibits tumor growth and improves survival in a transgenic mouse model of pancreatic islet cell tumors. ScientificWorldJournal, 2012. 2012: p. 529151.
29. Azimi A, et al., Silencing FLI or targeting CD13/ANPEP lead to dephosphorylation of EPHA2, a mediator of BRAF inhibitor resistance, and induce growth arrest or apoptosis in melanoma cells. Cell Death Dis, 2017 8(8): p. e3029. [PubMed: 29048432]
30. Nucera C, et al., Targeting BRAFV600E with PLX4720 displays potent antimigratory and anti-invasive activity in preclinical models of human thyroid cancer. Oncologist, 2011 16(3): p. 296–309. [PubMed: 21355020]
31. Hong DS, et al., Phase IB Study of Vemurafenib in Combination with Irinotecan and Cetuximab in Patients with Metastatic Colorectal Cancer with BRAFV600E Mutation. Cancer Discov, 2016 6(12): p. 1352–1365. [PubMed: 27729313]
32. Chakravarty D, et al., Small-molecule MAPK inhibitors restore radioiodine incorporation in mouse thyroid cancers with conditional BRAF activation. J Clin Invest, 2011 121(12): p. 4700–11. [PubMed: 22105174]
33. Jain RK and Booth MF, What brings pericytes to tumor vessels? J Clin Invest, 2003 112(8): p. 1134–6. [PubMed: 14561696]
34. Antonello ZA, et al., Vemurafenib-resistance via de novo RBM genes mutations and chromosome 5 aberrations is overcome by combined therapy with palbociclib in thyroid carcinoma with BRAF(V600E). Oncotarget, 2017 8(49): p. 84743–84760. [PubMed: 29156680]
35. Danysh BP, et al., Long-Term vemurafenib treatment drives inhibitor resistance through a spontaneous KRAS G12D mutation in a BRAF V600E papillary thyroid carcinoma model. Oncotarget, 2016.
36. Poulikakos PI, et al., RAF inhibitors transactivate RAF dimers and ERK signalling in cells with wild-type BRAF. Nature, 2010 464(7287): p. 427–30. [PubMed: 20179705]
37. Zhang X, et al., Thrombospondin-1 modulates vascular endothelial growth factor activity at the receptor level. FASEB J, 2009 23(10): p. 3368–76. [PubMed: 19528255]
38. Kazerounian S, Yee KO, and Lawler J, Thrombospondins in cancer. Cell Mol Life Sci, 2008 65(5): p. 700–12. [PubMed: 18193162]
39. Integrated genomic characterization of papillary thyroid carcinoma. Cell, 2014 159(3): p. 676–90. [PubMed: 25417114]

40. Cabanillas ME, et al., Thyroid Gland Malignancies. Hematol Oncol Clin North Am, 2015 29(6): p. 1123–43. [PubMed: 26568552]
41. Shibue T and Weinberg RA, EMT, CSCs, and drug resistance: the mechanistic link and clinical implications. Nat Rev Clin Oncol, 2017.
42. Dadu R, et al., Role of salvage targeted therapy in differentiated thyroid cancer patients who failed first-line sorafenib. J Clin Endocrinol Metab, 2014 99(6): p. 2086–94. [PubMed: 24628550]
43. Dvorak HF, Tumor Stroma, Tumor Blood Vessels, and Antiangiogenesis Therapy. Cancer J, 2015 21(4): p. 237–43. [PubMed: 26222073]
44. Zhu AX, et al., HCC and angiogenesis: possible targets and future directions. Nat Rev Clin Oncol, 2011 8(5): p. 292–301. [PubMed: 21386818]
45. Bollag G, et al., Vemurafenib: the first drug approved for BRAF-mutant cancer. Nat Rev Drug Discov, 2012 11(11): p. 873–86. [PubMed: 23060265]
46. Su F, et al., Resistance to selective BRAF inhibition can be mediated by modest upstream pathway activation. Cancer Res, 2012 72(4): p. 969–78. [PubMed: 22205714]
47. Lynch JM, et al., A thrombospondin-dependent pathway for a protective ER stress response. Cell, 2012 149(6): p. 1257–68. [PubMed: 22682248]
48. Young GD and Murphy-Ullrich JE, Molecular interactions that confer latency to transforming growth factor-beta. J Biol Chem, 2004 279(36): p. 38032–9. [PubMed: 15208302]
49. Calon A, et al., Dependency of colorectal cancer on a TGF-beta-driven program in stromal cells for metastasis initiation. Cancer Cell, 2012 22(5): p. 571–84. [PubMed: 23153532]
50. David CJ, et al., TGF-beta Tumor Suppression through a Lethal EMT. Cell, 2016 164(5): p. 1015–30. [PubMed: 26898331]
51. Massague J, TGFbeta signalling in context. Nat Rev Mol Cell Biol, 2012 13(10): p. 616–30. [PubMed: 22992590]
52. Taverna D and Hynes RO, Reduced blood vessel formation and tumor growth in alpha5-integrin-negative teratocarcinomas and embryoid bodies. Cancer Res, 2001 61(13): p. 5255–61. [PubMed: 11431367]
53. Caspani EM, et al., Glioblastoma: a pathogenic crosstalk between tumor cells and pericytes. PLoS One, 2014 9(7): p. e101402. [PubMed: 25032689]
54. Sweetwyne MT, et al., The calreticulin-binding sequence of thrombospondin 1 regulates collagen expression and organization during tissue remodeling. Am J Pathol, 2010 177(4): p. 1710–24. [PubMed: 20724603]
55. Nagy JA, et al., Permeability properties of tumor surrogate blood vessels induced by VEGF-A. Lab Invest, 2006 86(8): p. 767–80. [PubMed: 16732297]

## Statement of translational relevance

Metastatic, radioiodine refractory heterozygous $BRAF^{WT/V600E}$-PTC is resistant to targeted therapies and represents an unanswered clinical challenge. We show that combined therapy with vemurafenib and sorafenib *in vivo* does not provide therapeutic efficacy as compared to single agent treatments, likely due to tumor angiogenic activity in the microenvironment. Furthermore, we propose a novel model of drug resistance mediated by PTC microenvironment-associated pericytes via the TSP-1/TGFβ1 axis. Antagonizing the TSP-1/TGFβ1 axis may represent a novel therapeutic approach with translational applications for $BRAF^{WT/V600E}$-PTC resistant to targeted therapies. Finally, TSP-1 is a potential biomarker for assessing therapeutic response to $BRAF^{V600E}$ and TK inhibitors in patients with invasive $BRAF^{WT/V600E}$-PTC.

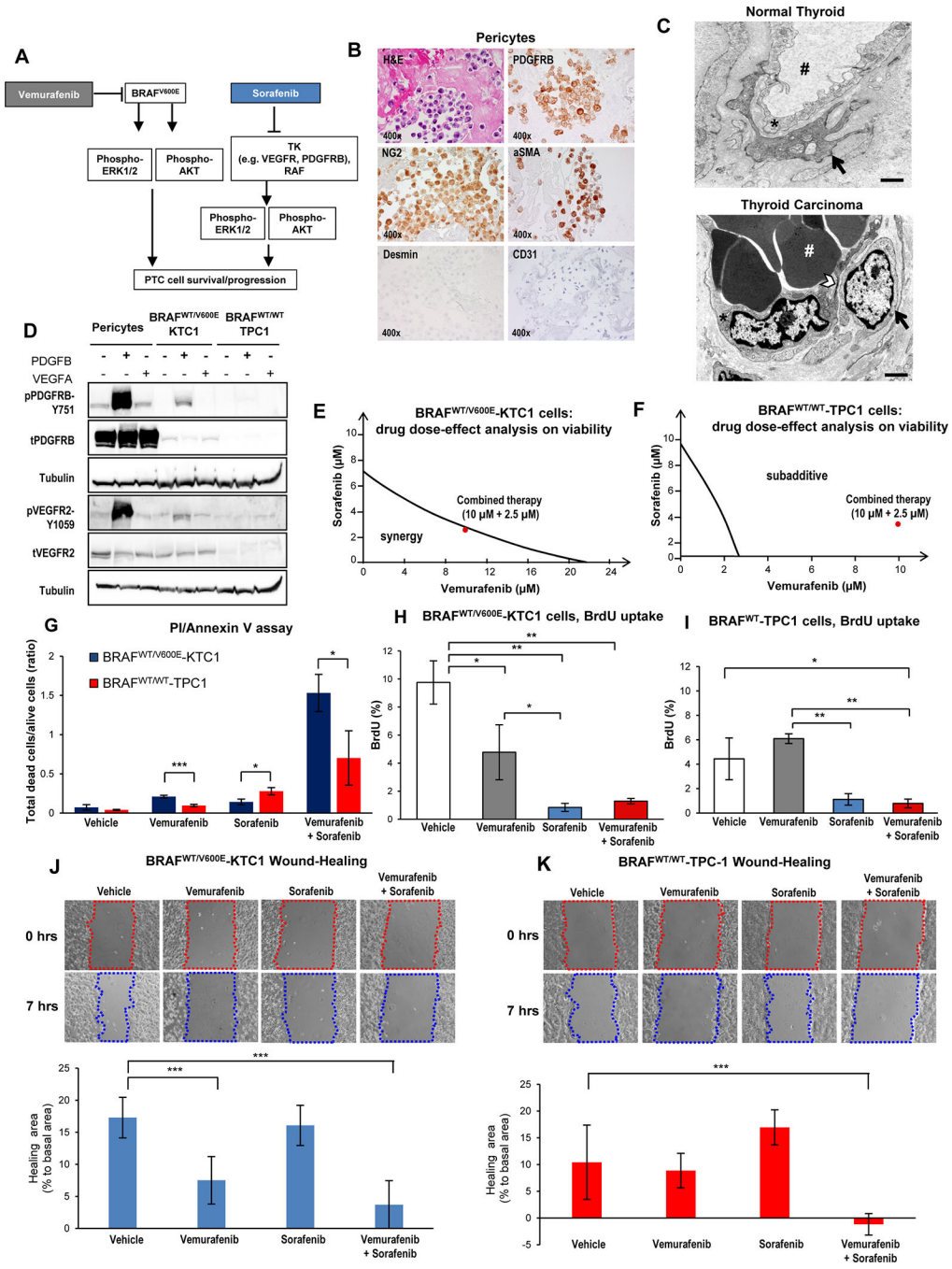


**Figure 1. Combined therapy with vemurafenib plus sorafenib induces stronger cell death compared to single agent treatment in PTC cells**

**(A)** Diagram of targeted therapy with $BRAF^{V600E}$ inhibitor and tyrosine kinase (TK) inhibitors against human invasive thyroid carcinoma cells harboring the heterozygous $BRAF^{V600E}$ mutation. **(B)** Immunocytochemistry and Hematoxylin-Eosin (H&E) stained sections of formalin-fixed paraffin-embedded (FFPE) cell blocks of representative human pericytes *in vitro*. Immunocytochemistry staining shows cytoplasmic to membranous staining with antibodies against PDGFRB, NG2, and αSMA. Desmin and CD31

immunostain was negative. **(C)** Representative transmission electron microscopy (TEM). Above: venule from normal human thyroid shows a typical endothelial cell (asterisk) with vascular lumen (pound sign) filled with plasma and enveloped by a pericyte (black arrow). A small pericyte (arrow) surrounds the abluminal surface of the endothelium. Below: in contrast, venule from a well-differentiated human thyroid carcinoma (n=3) shows an endothelial cell (asterisk) with large, activated nucleus and thinned cytoplasm (arrowhead) enveloped by an activated pericyte (black arrow). Vascular lumen is filled with densely packed red blood cells (white pound sign) and with little plasma present, which is a characteristic sign [55] of vascular permeability to plasma. Scale bar size=500 nm. **(D)** Western blotting analysis (protein loading: 70 μg/lane) of protein expression levels in human $BRAF^{WT}$-pericytes, $BRAF^{WT/V600E}$-KTC1 and $BRAF^{WT/WT}$-TPC1 cells at 20 minutes post stimulation with VEGF (20 ng/mL) or PDGFB (20 ng/mL). Both tubulin blots are different and derive from two different membranes. These results were validated by two independent experiments. **(E-F)** Visualization of drug combinations: dose-effect analysis of combined therapy with vemurafenib plus sorafenib vs. vehicle on $BRAF^{WT/V600E}$-KTC1 and $BRAF^{WT/WT}$-TPC1 cell viability (cells were grown in 0.2% FBS DMEM growth medium during treatment). Each point represents the mean of three replicates from two independent measurements. This method uses the dose-effect data of the individual drugs and drugs combined doses. The area of synergy or sub-additive effects is distinguished by the line (isobole curve), which indicates additive effects. The red dot highlights the best dose-effect using combined treatment with vemurafenib plus sorafenib. **(G)** Quantification of cell death by annexin V and propidium iodide (PI) dual staining assay in $BRAF^{WT/V600E}$-KTC1 and $BRAF^{WT/WT}$-TPC1 cells at 48 hrs treatment with DMSO (vehicle), 10 μM vemurafenib, 2.5 μM sorafenib and combined therapy with 10 μM vemurafenib plus 2.5 μM sorafenib; cells were grown in 0.2% FBS DMEM growth medium during treatment. These data represent the average ± standard deviation (error bars) of two independent replicate measurements (n=3 for each condition, *p<0.05, **p<0.01, ***p<0.001). (H-I) Quantification of cell proliferation by combined BrdU (5-bromo-2-deoxyuridine) pulse/PI (propidium iodide) by flow cytometry analysis of $BRAF^{WT/V600E}$-KTC1 and $BRAF^{WT/WT}$-TPC1 cells at 48 hrs treatment with DMSO (vehicle), 10 μM vemurafenib, 2.5 μM sorafenib and combined therapy with 10 μM vemurafenib plus 2.5 μM sorafenib; cells were grown in 0.2% FBS DMEM growth medium during treatment. These data represent the average ± standard deviation (error bars) of two independent replicate measurements (*p<0.05, **p<0.01). (J-K) Quantification of $BRAF^{WT/V600E}$-KTC1 and $BRAF^{WT/WT}$-TPC1 cell motility was analyzed by wound-healing assay. Cells were grown in 0.2% FBS DMEM growth medium during treatment. Images were captured at 0 and 7 hours after culture scratch. These data are representative of two independent replicate measurements calculating percentage of healing area at 7 hrs compared to 0 hrs (basal area) for each condition. Statistical analysis was performed comparing drug treatments vs. vehicle (**p<0.01, ***p<0.001).

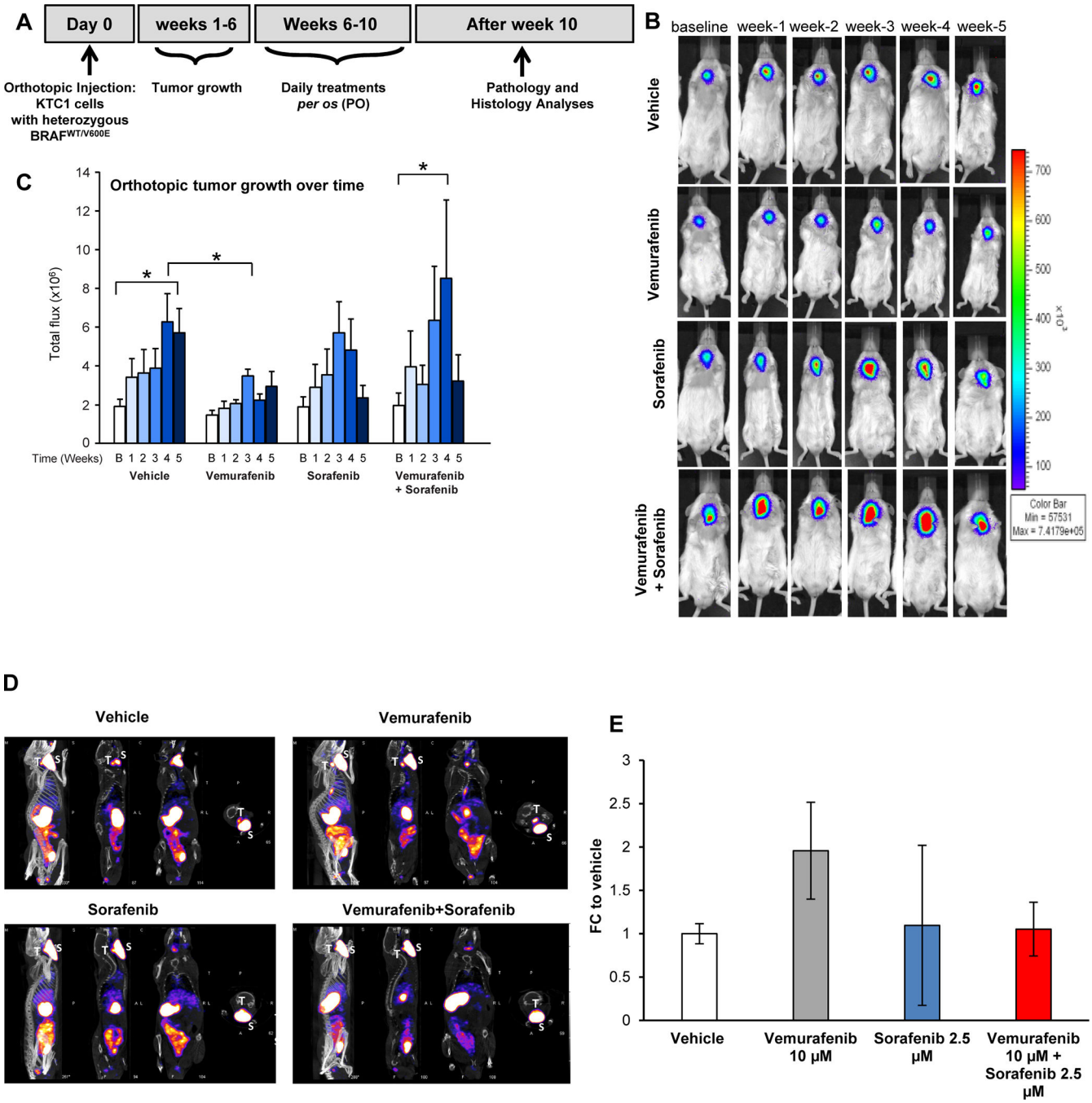


**Figure 2. Effects of targeted therapy with vemurafenib and sorafenib in a late intervention model of an orthotopic mouse using PTC-derived KTC1 cells harboring the heterozygous BRAF$^{V600E}$ mutation.**

**A)** Experimental design of an *in vivo* late intervention orthotopic preclinical model using BRAF$^{WT/V600E}$-KTC1 cells derived from a patient with invasive PTC harboring the heterozygous BRAF$^{WT/V600E}$ mutation. Human BRAF$^{WT/V600E}$-KTC1 cells, engineered to express luciferase, were implanted in 20 nine-week-old male NSG mice, which were then treated with vemurafenib, sorafenib, combined therapy, or vehicle (n=5 for each experimental condition). Their orthotopic tumors were evaluated by histology and

bioluminiscence imaging. Either vehicle, vemurafenib (100 mg/kg, one time daily), sorafenib (30 mg/kg, one time daily), or combined therapy vemurafenib (100 mg/kg, one time daily) plus sorafenib (30 mg/kg, one time daily) treatments were begun at 6 weeks post-tumor implantation, and the response to drugs was evaluated weekly for 5 weeks. **(B)** BLI (bioluminescence imaging, emission of photons/second) analysis for tumor growth assessment (by luciferase signal) in mice treated daily with vehicle, vemurafenib, sorafenib, or combined therapy for five weeks. **(C)** Total flux analysis of BLI (emission of photons/second) and distribution of data showed that five weeks of vemurafenib treatment resulted in significantly lower orthotopic tumor growth than in controls (vehicle treatment) (*$p<0.05$, Mann-Whitney test). Sorafenib therapy was fluctuant and resulted in a smaller reduction in tumor growth. Combined therapy showed a rising trend in tumor growth at week 4 followed by a decrease at week 5 vs. vehicle treatment. B=baseline. **(D)** MicroSPECT/CT representative images of results plotted in E. T= mouse thyroids, S= mouse salivary glands. **(E)** Quantification of technetium-99 ($^{99m}$Tc) uptake in BRAF$^{WT/V600E}$-positive KTC1 orthotopic tumors based on the standardized uptake value (SUV) calculated by tissue radioactivity concentration/injected activity/body weight in grams and obtained by combining CT (Computed Tomography) and microSPECT (Single Photon Emission Computed Tomography) imaging analysis performed in mice at four weeks post-treatment with vehicle (n=2), vemurafenib (100 mg/kg, one time daily) (n=2), sorafenib (30 mg/kg, one time daily) (n=2), or combined therapy with vemurafenib (100 mg/kg, one time daily) plus sorafenib (30 mg/kg, one time daily) (n=2). These data represent the fold change (FC) ± standard deviation (error bars) compared to the vehicle treatment.

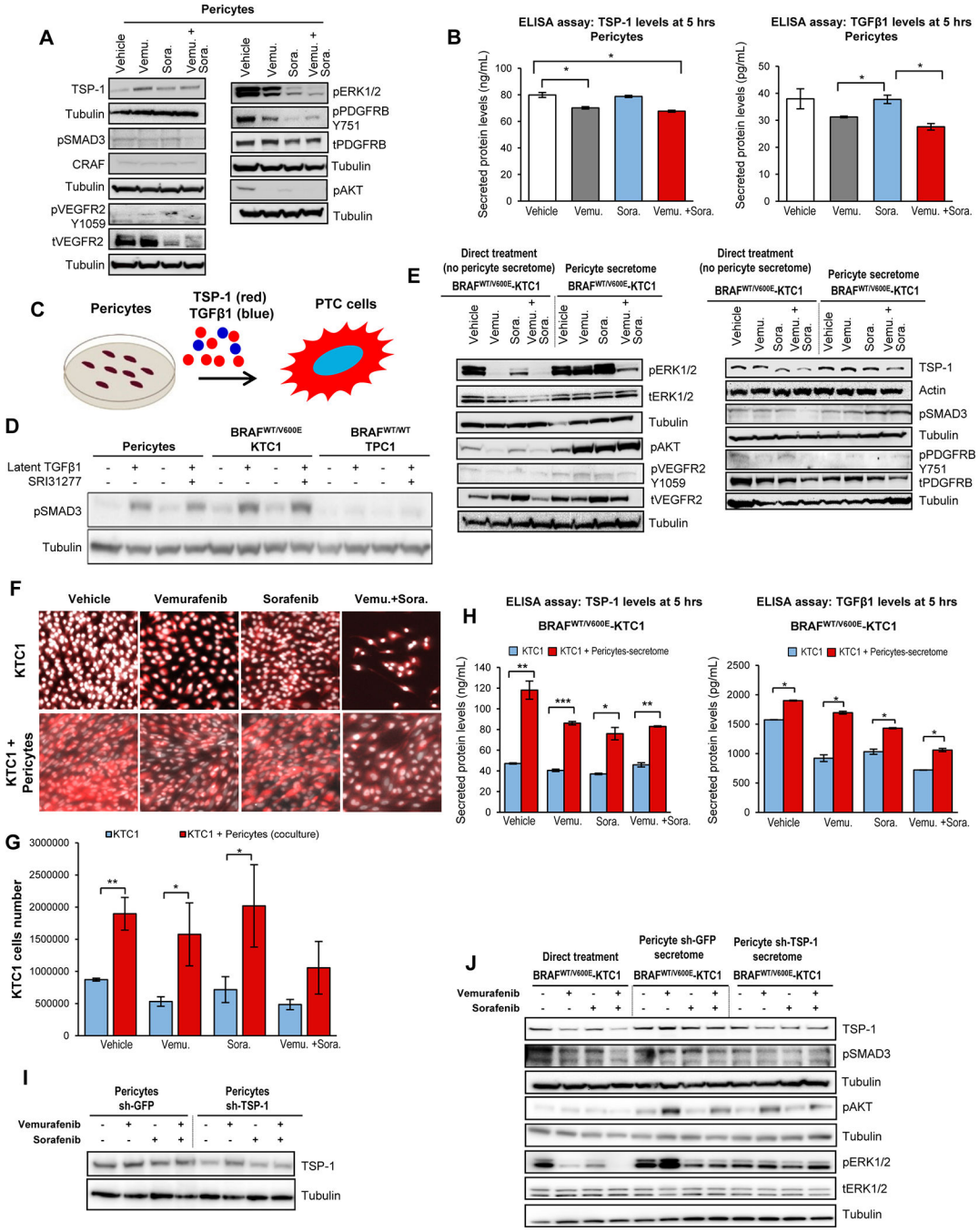


**Figure 3. Model of co-culture with PTC patient-derived cells harboring the heterozygous BRAF$^{V600E}$ mutation and pericytes reveals resistance to BRAF$^{V600E}$ and tyrosine kinase inhibitors via the TSP-1/TGFβ1 axis.**

**A)** Western blot analysis of proteins expression levels in pericytes at 5 hrs treatment with DMSO (vehicle), 10 μM vemurafenib, 2.5 μM sorafenib and combined therapy with 10 μM vemurafenib plus 2.5 μM sorafenib. These results were validated by three independent replicate measurements. Cells were grown in 0.2% FBS DMEM growth medium during treatment. **B)** Measurements of secreted TSP-1 and TGFβ1 total protein levels in pericytes treated for 5 hrs with DMSO (vehicle), 10 μM vemurafenib, 2.5 μM sorafenib, or combined

therapy with 10 μM vemurafenib plus 2.5 μM sorafenib, in the presence of 0.2% FBS DMEM growth medium. The secretome (0.2% FBS DMEM cell growth medium enriched by cell-derived secreted protein factors) was collected and protein levels (ng/mL or pg/mL) were determined by ELISA (enzyme-linked immunosorbent assay). Secreted protein levels were normalized to cell growth medium (DMEM supplemented with 0.2% FBS) which was measured to determine subtracted background. These data represent the average ± standard deviation (error bars) of two independent replicate measurements (*$p<0.05$). **C)** Diagram of secreted factors (i.e. TSP-1, TGFβ1) derived from human pericytes treated for 5 hrs with vehicle, 10 μM vemurafenib, 2.5 μM sorafenib, or combined therapy with 10 μM vemurafenib plus 2.5 μM sorafenib grown in the presence of 0.2% FBS DMEM growth medium as shown in A; secreted factors represent pericyte conditioned medium to treat PTC cells. **D)** Western blot analysis of pSMAD3 proteins expression levels in human pericytes, $BRAF^{WT/V600E}$-KTC1 and $BRAF^{WT/WT}$-TPC1 cells treated for 5 hrs with vehicle, recombinant human latent TGFβ1 protein (2 ng/mL), 10 μM SRI31277, or recombinant human latent TGFβ1 protein (2 ng/mL) plus 10 μM SRI31277 in the presence of 0.2% FBS DMEM growth medium. **E)** Western blot analysis of proteins expression levels in $BRAF^{WT/V600E}$-KTC1 cells at 5 hrs direct treatment (without pericytes conditioned medium; cells were grown in 0.2% FBS DMEM growth medium during treatment) with DMSO (vehicle), 10 μM vemurafenib, 2.5 μM sorafenib, or combined therapy with 10 μM vemurafenib plus 2.5 μM sorafenib; or 5 hrs treatments with pericyte-derived conditioned medium (defined secretome) treated with DMSO (vehicle), 10 μM vemurafenib, 2.5 μM sorafenib or combined therapy with 10 μM vemurafenib plus 2.5 μM sorafenib as shown in A. These results were validated by three independent replicates. **F)** Fluorescence imaging for fixed $BRAF^{WT/V600E}$-$KTC1^{mCherry}$ cells alone (highlighted by mCherry and Hoechst staining, with red and white signal, respectively) or co-cultured with pericytes (highlighted by mCherry (red signal) specific to label KTC1 cells and Hoechst (white signal) staining to label both KTC1 cells and pericytes). KTC1 cells or co-cultures were treated for 48 hrs with DMSO (vehicle), 10 μM vemurafenib, 2.5 μM sorafenib, or combined therapy with 10 μM vemurafenib plus 2.5 μM sorafenib. Cells were grown in 0.2% FBS DMEM growth medium during treatment. **G)** Quantification of only $BRAF^{WT/V600E}$-$KTC1^{mCherry}$ cells reported in F. These data represent the average ± standard deviation (error bars) of three independent replicates (*$p<0.05$, **$p<0.01$). **H)** Measurements of secreted TSP-1 and TGFβ1 total protein levels in: $BRAF^{WT/V600E}$-KTC1 cells directly treated (without pericyte conditioned medium, blue bars) for 5 hrs with DMSO (vehicle), 10 μM vemurafenib, 2.5 μM sorafenib, or combined therapy with 10 μM vemurafenib plus 2.5 μM sorafenib in the presence of 0.2% FBS DMEM growth medium; and in $BRAF^{WT/V600E}$-KTC1 cells treated for 5 hrs with pericyte-derived conditioned medium (secretome, red bars) treated with DMSO (vehicle), 10 μM vemurafenib, 2.5 μM sorafenib, or combined therapy with 10 μM vemurafenib plus 2.5 μM sorafenib, in the presence of 0.2% FBS DMEM growth medium. The secretome (pericyte-derived conditioned medium) was collected and protein levels (ng/mL or pg/mL) were determined by ELISA (enzyme-linked immunosorbent assay). Secreted protein levels were normalized to cell growth medium (DMEM supplemented with 0.2% FBS) that was measured to determine subtracted background. These data represent the average ± standard deviation (error bars) of two independent replicates (*$p<0.05$, **$p<0.01$, ***$p<0.001$). **I)** Western blot analysis of protein expression levels in sh-GFP (control) or sh-TSP-1 pericytes

at 5 hrs treatment with DMSO (vehicle), 10 μM vemurafenib, 2.5 μM sorafenib and combined therapy with 10 μM vemurafenib plus 2.5 μM sorafenib in the presence of 0.2% FBS DMEM growth medium. These results were validated by two independent replicates. **J)** Western blot analysis of protein expression levels in $BRAF^{WT/V600E}$-KTC1 cells at 5 hrs direct treatment (without pericyte-derived conditioned medium) with DMSO (vehicle), 10 μM vemurafenib, 2.5 μM sorafenib, or combined therapy with 10 μM vemurafenib plus 2.5 μM sorafenib in the presence of 0.2% FBS DMEM growth medium; or 5 hrs treatments with sh-GFP (control) or sh-TSP-1 pericyte-derived conditioned medium (secretome) treated with DMSO (vehicle), 10 μM vemurafenib, 2.5 μM sorafenib, or combined therapy with 10 μM vemurafenib plus 2.5 μM sorafenib as shown in I. These results were validated by 2 independent replicates.

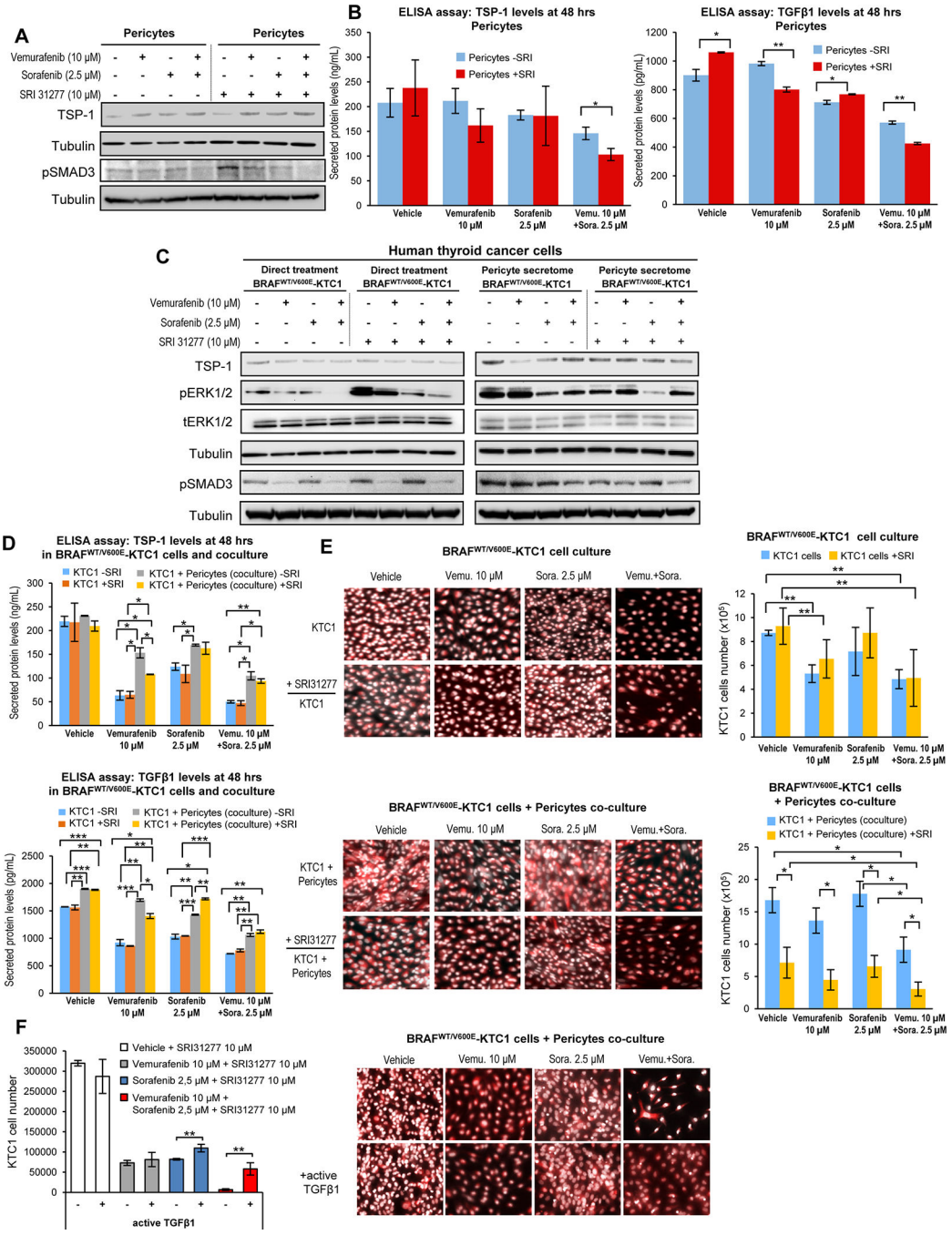


**Figure 4. The SRI31277 peptide overcomes resistance to vemurafenib plus sorafenib therapy in PTC-derived cells harboring the heterozygous BRAF$^{V600E}$ mutation.**

**A)** Western blot analysis of proteins expression levels in pericytes at 5 hrs treatment with DMSO (vehicle), 10 μM vemurafenib, 2.5 μM sorafenib and combined therapy with 10 μM vemurafenib plus 2.5 μM sorafenib in the presence or absence of the SRI31277 peptide that blocks TSP-1/TGFβ1 activation (cells were grown in 0.2% FBS DMEM growth medium during treatment). These results were validated by two measurements. **B)** Measurements of secreted TSP-1 and TGFβ1 total protein levels in pericytes treated for 48 hrs with DMSO

(vehicle), 10 μM vemurafenib, 2.5 μM sorafenib, or combined therapy with 10 μM vemurafenib plus 2.5 μM sorafenib (cells were grown in 0.2% FBS DMEM growth medium during treatment) in the presence or absence of the SRI31277 peptide (10 μM). The secretome (0.2% FBS DMEM growth medium enriched by cell-derived secreted protein factors) was collected and protein levels (ng/mL or pg/mL) were determined by ELISA (enzyme-linked immunosorbent assay). Secreted protein levels were normalized to cell growth medium (DMEM supplemented with 0.2% FBS) which was measured to determine subtracted background. These data represent the average ± standard deviation (error bars) of 2 independent replicate measurements (*p<0.05, **p<0.01). **C)** Western blot analysis of proteins expression levels in $BRAF^{WT/V600E}$-KTC1 cells at 5 hrs direct treatment with DMSO (vehicle), 10 μM vemurafenib, 2.5 μM sorafenib, or combined therapy with 10 μM vemurafenib plus 2.5 μM sorafenib in the presence or absence of the SRI31277 peptide; or 5 hrs treatments with pericyte-derived secretome treated with DMSO (vehicle), 10 μM vemurafenib, 2.5 μM sorafenib or combined therapy with 10 μM vemurafenib plus 2.5 μM sorafenib as shown in A in the presence or absence of the SRI31277 peptide. Cells were grown in 0.2% FBS DMEM growth medium during treatment. These results were validated by two independent replicate measurements. **D)** Measurements of secreted TSP-1 and TGFβ1 total protein levels in both $BRAF^{V600E}$-KTC1 cells and co-culture with $BRAF^{WT/V600E}$-$KTC1^{mCherry}$ cells and pericytes treated for 48 hrs with DMSO (vehicle), 10 μM vemurafenib, 2.5 μM sorafenib, or combined therapy with 10 μM vemurafenib plus 2.5 μM sorafenib in the presence or absence of the SRI31277 peptide (10 μM); cells were grown in 0.2% FBS DMEM growth medium during treatment. The secretome (0.2% FBS DMEM cell growth medium enriched by cell-derived secreted protein factors) was collected and protein levels (ng/mL or pg/mL) were determined by ELISA (enzyme-linked immunosorbent assay). Secreted protein levels were normalized to cell growth medium (DMEM supplemented with 0.2% FBS) that was measured to determine subtracted background. These data represent the average ± standard deviation (error bars) of 2 independent replicate measurements (*p<0.05, **p<0.01, ***p<0.001). **E)** Fluorescence imaging for fixed $BRAF^{WT/V600E}$-$KTC1^{mCherry}$ cells (highlighted by mCherry and Hoechst staining, with red and white signal, respectively) treated for 48 hrs with DMSO (vehicle), 10 μM vemurafenib, 2.5 μM sorafenib, or combined therapy with 10 μM vemurafenib plus 2.5 μM sorafenib in the presence or absence of the SRI31277 peptide (10 μM); cells were grown in 0.2% FBS DMEM growth medium during treatment. Quantification of only $BRAF^{WT/V600E}$-$KTC1^{mCherry}$ cells number is reported in the histogram. Fluorescence imaging for fixed co-culture with $BRAF^{WT/V600E}$-$KTC1^{mCherry}$ cells (highlighted by mCherry and Hoechst staining, with red and white signal, respectively) and pericytes (highlighted by Hoechst staining, white signal) treated for 48 hrs with DMSO (vehicle), 10 μM vemurafenib, 2.5 μM sorafenib, or combined therapy with 10 μM vemurafenib plus 2.5 μM sorafenib in the presence or absence of the SRI31277 peptide (10 μM); cells were grown in 0.2% FBS DMEM growth medium during treatment. Quantification of only $BRAF^{WT/V600E}$-$KTC1^{mCherry}$ cells number is reported in the histogram. These data represent the average ± standard deviation (error bars) of three independent replicate measurements (*p<0.05, **p<0.01). **F)** Fluorescence imaging for fixed co-culture with $BRAF^{WT/V600E}$-$KTC1^{mCherry}$ cells (highlighted by mCherry and Hoechst staining, with red and white signal, respectively) and pericytes (highlighted by Hoechst staining, white signal)

treated for 48 hrs with DMSO (vehicle), 10 μM vemurafenib, 2.5 μM sorafenib, or combined therapy with 10 μM vemurafenib plus 2.5 μM sorafenib in the presence or absence of the SRI31277 peptide (10 μM); cells were grown in 0.2% FBS DMEM growth medium during treatment. Cell coculture was stimulated every 8 hrs for 48 hrs with recombinant human active TGFβ1 (7.75 ng/500μL in 24 well dishes) and compared to cell coculture without recombinant human active TGFβ1 as a control. Quantification of only $BRAF^{WT/V600E}$-$KTC1^{mCherry}$ cells numbers are reported in the histogram. These data represent the average ± standard deviation (error bars) of three replicate measurements (**$p<0.01$).

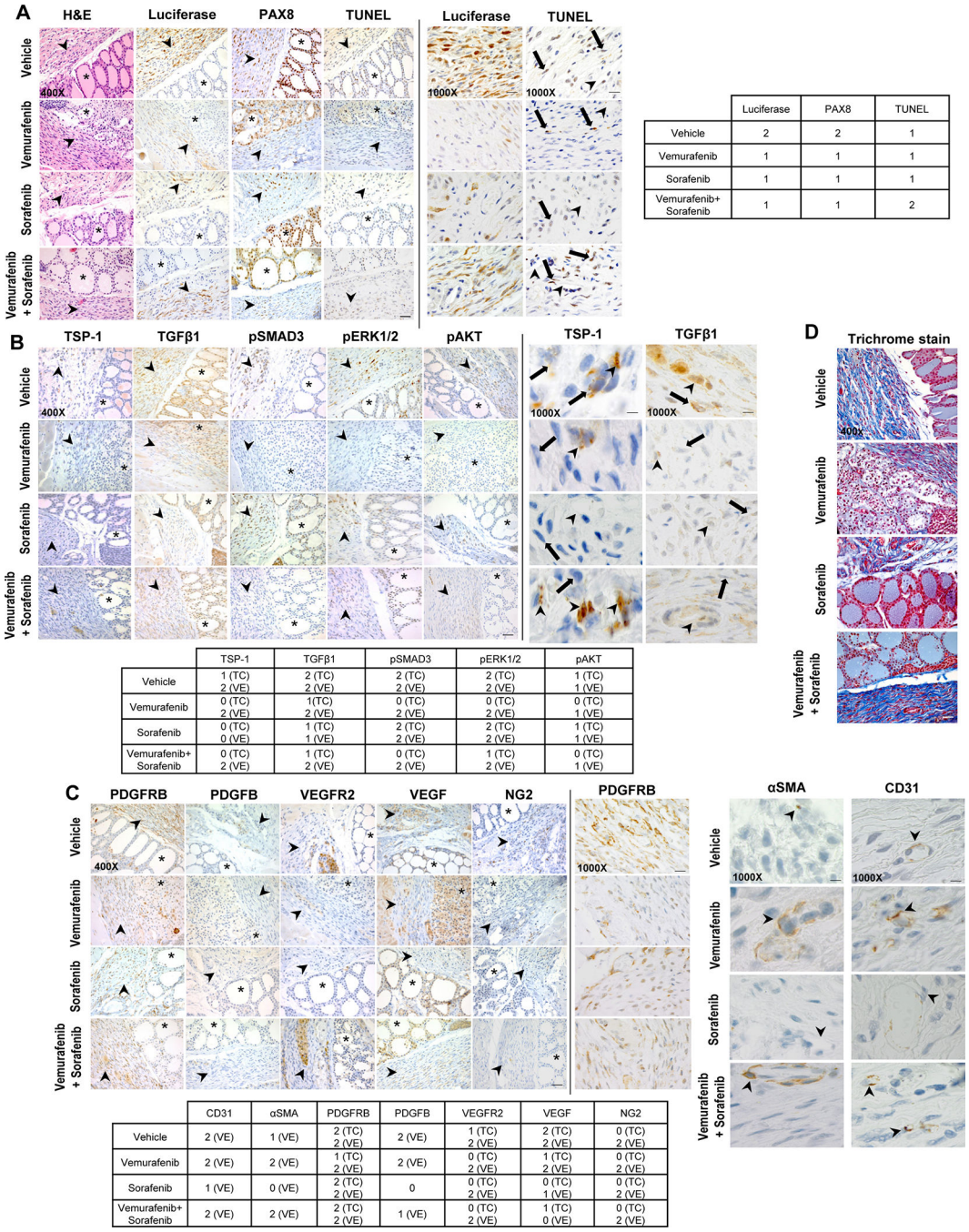


| | Luciferase | PAX8 | TUNEL |
|---|---|---|---|
| Vehicle | 2 | 2 | 1 |
| Vemurafenib | 1 | 1 | 1 |
| Sorafenib | 1 | 1 | 1 |
| Vemurafenib+ Sorafenib | 1 | 1 | 2 |

| | TSP-1 | TGFβ1 | pSMAD3 | pERK1/2 | pAKT |
|---|---|---|---|---|---|
| Vehicle | 1 (TC)<br>2 (VE) | 2 (TC)<br>2 (VE) | 2 (TC)<br>2 (VE) | 2 (TC)<br>2 (VE) | 1 (TC)<br>1 (VE) |
| Vemurafenib | 0 (TC)<br>2 (VE) | 1(TC)<br>2 (VE) | 0 (TC)<br>2 (VE) | 0 (TC)<br>2 (VE) | 0 (TC)<br>1 (VE) |
| Sorafenib | 0 (TC)<br>0 (VE) | 1 (TC)<br>1 (VE) | 2 (TC)<br>2 (VE) | 2 (TC)<br>2 (VE) | 1 (TC)<br>1 (VE) |
| Vemurafenib+ Sorafenib | 0 (TC)<br>2 (VE) | 1 (TC)<br>2 (VE) | 0 (TC)<br>2 (VE) | 1 (TC)<br>2 (VE) | 0 (TC)<br>1 (VE) |

| | CD31 | αSMA | PDGFRB | PDGFB | VEGFR2 | VEGF | NG2 |
|---|---|---|---|---|---|---|---|
| Vehicle | 2 (VE) | 1 (VE) | 2 (TC)<br>2 (VE) | 2 (VE) | 1 (TC)<br>2 (VE) | 2 (TC)<br>2 (VE) | 0 (TC)<br>2 (VE) |
| Vemurafenib | 2 (VE) | 2 (VE) | 1 (TC)<br>2 (VE) | 2 (VE) | 0 (TC)<br>2 (VE) | 1 (TC)<br>2 (VE) | 0 (TC)<br>2 (VE) |
| Sorafenib | 1 (VE) | 0 (VE) | 2 (TC)<br>2 (VE) | 0 | 0 (TC)<br>2 (VE) | 0 (TC)<br>1 (VE) | 0 (TC)<br>2 (VE) |
| Vemurafenib+ Sorafenib | 2 (VE) | 2 (VE) | 2 (TC)<br>2 (VE) | 1 (VE) | 0 (TC)<br>2 (VE) | 1 (TC)<br>0 (VE) | 0 (TC)<br>2 (VE) |

**Figure 5. Immunohistochemical analysis of angiogenesis factors and TSP-1/TGFβ1 expression in the orthotopic human PTC harboring the heterozygous BRAF$^{V600E}$ mutation treated with targeted therapy.**

**A)** BRAF$^{WT/V600E}$-positive human KTC1 orthotopic tumor growth *in vivo* in the late intervention mouse model described in 2A-C. Control mice (H&E, luciferase and PAX8 stain) showed tumor growth within a circumscribed area, with mixed spindled features and atypical cells. Magnifications: 400x or 1000x. Scale bars are shown in the lower or upper panel for the 400x and 1000x photomicrographs, respectively: 100 microns (400x images) or 50 microns (1000x images). Arrowhead (shown in the left panel for the 400x

photomicrographs) highlights orthotopic KTC1 tumor area, asterisk highlights mouse normal thyroid follicles area. Right panel for the 1000x photomicrographs: arrows mark tumor cells and arrowheads mark VE=vascular/endothelial compartment. Abbreviations: H&E, hematoxylin and eosin. Terminal deoxynucleotidyl transferase dUTP nick end labeling (TUNEL) IHC (immunohistochemistry) for detecting DNA fragmentation/dead cells. Luciferase, PAX8 and TUNEL stains were assessed semi-quantitatively using the following scoring method: 0 (negative), 1 (<50% positive cells), and 2 (≥50% positive cells). **B)** Immunohistochemical protein expression of TSP-1, TGFβ1, phospho(p)-SMAD3, pERK1/2, and pAKT in $BRAF^{WT/V600E}$-KTC1 orthotopic tumors mice at week 5 post-treatment with vehicle, vemurafenib (100 mg/kg, one time daily), sorafenib (30 mg/kg, one time daily), or combined therapy with vemurafenib (100 mg/kg, one time daily) plus sorafenib (30 mg/kg, one time daily). Arrowhead (shown in the left panel for the 400x photomicrographs) highlights orthotopic KTC1 tumor area, asterisk highlights mouse normal thyroid follicles area. Right panel for the 1000x photomicrographs: arrows mark tumor cells and arrowheads mark VE=vascular/endothelial compartment. IHC stains were assessed semi-quantitatively using the following scoring method: 0 (negative), 1 (<50% positive cells), and 2 (≥50% positive cells). VE= vascular/endothelial compartment. Magnifications: 400x or 1000x. Scale bars are shown in the lower or upper panel for the 400x and 1000x photomicrographs, respectively: 100 microns (400x images) or 50 microns (1000x images). **C)** Immunohistochemical protein expression of CD31, αSMA, PDGFRB, PDGFB, VEGFR2, VEGF, and NG2 in $BRAF^{WT/V600E}$-KTC1 orthotopic tumors mice at week 5 post-treament with vehicle, vemurafenib (100 mg/kg, one time daily), sorafenib (30 mg/kg, one time daily), or combined therapy with vemurafenib (100 mg/kg, one time daily) plus sorafenib (30 mg/kg, one time daily). Arrowhead (shown in the left panel for the 400x photomicrographs) highlights orthotopic KTC1 tumor area, asterisk highlights mouse normal thyroid follicles area. Right panel for the αSMA and CD31 1000x photomicrographs: arrowheads mark VE=vascular/endothelial compartment (i.e. microvessels). IHC stains were assessed semi-quantitatively using the following scoring method: 0 (negative), 1 (<50% positive cells), and 2 (≥50% positive cells). VE= vascular/endothelial compartment. Magnifications: 400x or 1000x. Scale bars are shown in the lower or upper panel for the 400x and 1000x photomicrographs, respectively: 100 microns (400x images) or 50 microns (1000x images). **D)** Trichrome staining highlights the intratumoral abundant amount of collagen deposition (blue staining) in $BRAF^{WT/V600E}$-KTC1 orthotopic tumors mice at week 5 post-treatment with vehicle, vemurafenib (100 mg/kg, one time daily), sorafenib (30 mg/kg, one time daily), or combined therapy with vemurafenib (100 mg/kg, one time daily) plus sorafenib (30 mg/kg, one time daily). Magnification: 400x. Scale bar is shown on the bottom photomicrograph: 100 microns (400x images).

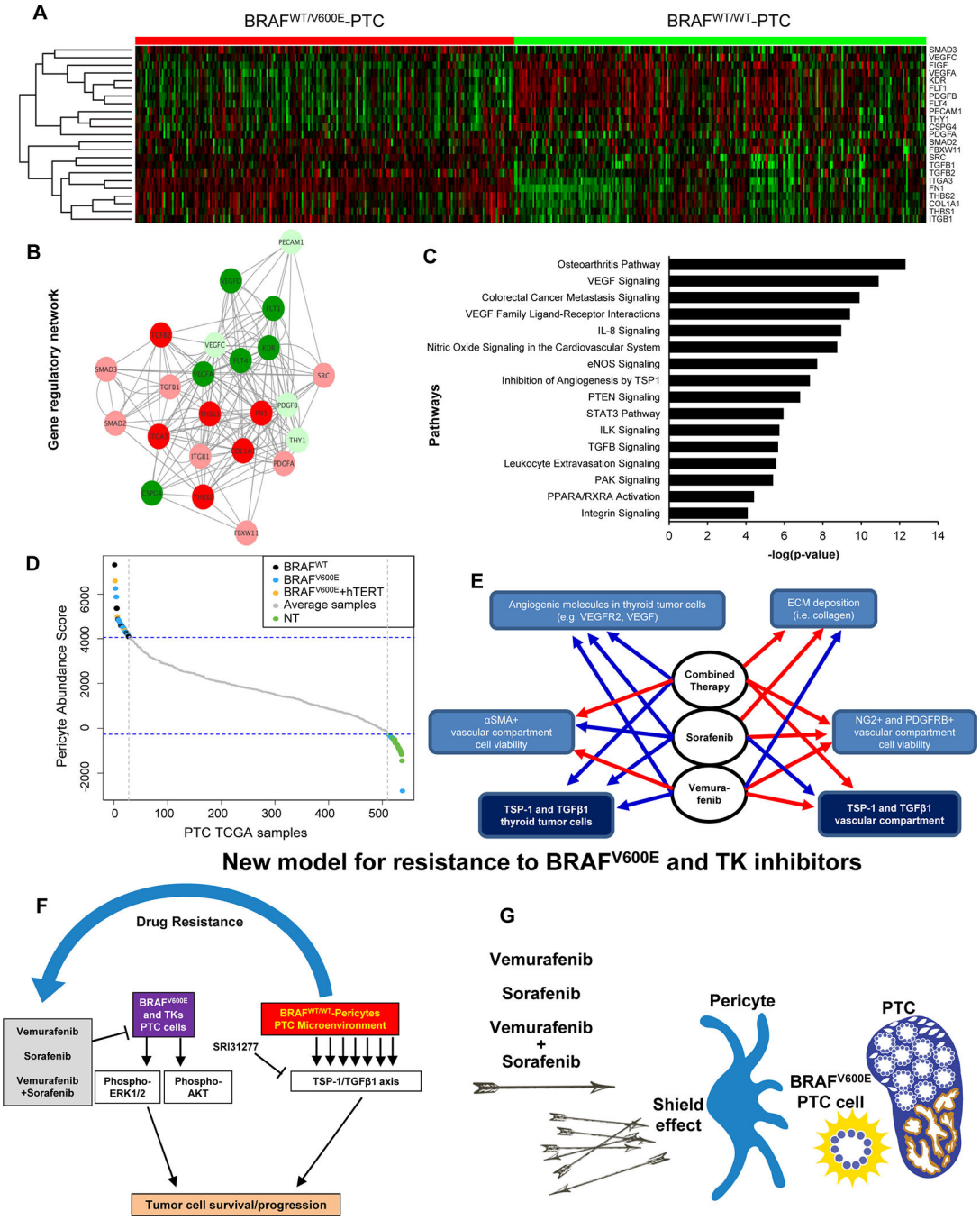


**Figure 6. TSP-1 (THBS1) gene regulatory networks and pericytes abundance in BRAF$^{WT/V600E}$-PTC versus BRAF$^{WT/WT}$-PTC clinical samples.**

**(A)** In the heatmap, rows depict differentially expressed genes and columns depict BRAF$^{WT/V600E}$-PTC vs. BRAF$^{WT/WT}$-PTC (PTC TCGA data base) samples. The relative expression level of genes is shown using a color scale. Colors indicate standardized values (green represents gene down-regulation and red represents gene up-regulation). **(B)** THBS1 (TSP-1) regulatory networks with genes differentially expressed in BRAF$^{V600E}$-PTC vs. BRAF$^{WT}$-PTC human samples (PTC TCGA data base) built up by Cytoscape. Each node

represents a gene and each edge represents the interaction between the genes. We observed that there is a significant interaction between the differentially expressed genes that are identified from $BRAF^{WT/V600E}$-PTC vs. $BRAF^{WT/WT}$-PTC human samples analysis. The co-expression analysis for these genes was performed on the basis of PTC TCGA data (interactions with p-value <0.05 from correlation test were considered significant). Image shows genes that depict significant interaction with TSP-1 or TGFβ1. Circles indicate genes deregulated in $BRAF^{WT/WT}$-PTC vs $BRAF^{WT/V600E}$-PTC samples; the color intensity corresponds to the extent of upregulation/downregulation based on the $log_2$FC values. **(C)** Pathways enrichment analysis for significantly differentially expressed genes shown in (A) in $BRAF^{WT/V600E}$-PTC vs. $BRAF^{WT/WT}$-PTC. The significance of effect/enrichment on pathways is shown along x-axis as $-log_{10}$ p-value. For pathways analysis: $-Log_{10}$ p-value 1.3= p-value= 0.05; $-log_{10}$ p-value 2= p-value= 0.01; $-log_{10}$ p-value 3= p-value= 0.001; $-log_{10}$ p-value 4= p-value=0.0001. **(D)** Plot of the pericytes abundance calculated by the pericytes abundance score in normal thyroid (NT) samples, $BRAF^{WT/V600E}$-PTC, PTC harboring both $BRAF^{V600E}$ and hTERT mutations, and $BRAF^{WT/WT}$-PTC samples (PTC TCGA data base) arranged in the order of their scores from highest to lowest. Only the 5% most pericytes enriched samples and the 5% least pericytes enriched samples are highlighted in color with the rest of the average samples shown in grey. The color code is green for NT samples, blue for $BRAF^{WT/V600E}$-PTC; black for $BRAF^{WT/WT}$-PTC, and orange for PTC with $BRAF^{WT/V600E}$ and hTERT mutations. **(E)** Flow chart that summarizes effects of vemurafenib, sorafenib, or combined therapy on the angiogenic molecules expression, collagen deposition, and TSP-1/TGFβ1/SMAD3 expression in the $BRAF^{WT/V600E}$-KTC1 orthotopic tumor cells and vessels compartment (see Fig.5). Blue line=down-regulation/ inhibitory effects. ECM=extracellular matrix. Red line=no inhibitory effects. **(F-G)** Overview of treatment with vemurafenib, sorafenib, or combined therapy. Combined therapy determines cell death in thyroid tumor cells; role of pericytes which might trigger resistance to these agents via the TSP1/TGFβ1 axis.